LOCKHEED MARTIN ENERGY RESEARCH LIBRARIES
3 4456 0514451 8

CENTRAL RESEARCH LIBRARY
DOCUMENT COLLECTION

OAK RIDGE NATIONAL LABORATORY
CENTRAL RESEARCH LIBRARY
DOCUMENT COLLECTION
LIBRARY LOAN COPY
DO NOT TRANSFER TO ANOTHER PERSON
If you wish someone else to see this document, send in name with document and the library will arrange a loan.

OAK RIDGE NATIONAL LABORATORY
operated by
UNION CARBIDE CORPORATION
for the
U. S. ATOMIC ENERGY COMMISSION

ORNL-TM-3379
cy. 155
DATE - April 1971

Physics Division

KEV NEUTRON CAPTURE GAMMA RAY SPECTRA

J. R. Bird,† I. Bergqvist,‡ J. A. Biggerstaff,
J. H. Gibbons, and W. M. Good

Abstract

Techniques are described for using a 9" x 12" NaI detector to measure pulse height spectra for gamma rays from the capture of 10-100 keV neutrons generated by a pulsed Van de Graaff beam. Pulse height spectra are given for capture in 36 elements or separated isotopes. In many cases, tabulated gamma ray intensities are compared with results for thermal neutron capture. In a few cases the excitation functions for particular gamma rays are included. The experimental work described was carried out at ORNL during the period 1961-1963 and some of the results have been presented in previous publications. This compilation summarizes all the spectra and intensities measured during that period.

---

†Visiting scientist from AERE, Harwell, England. Now at AAEC Research Establishment, Lucas Heights, N.S.W., Australia.

‡Visiting scientist from the Research Institute of National Defense, Stockholm, Sweden. Now at University of Lund, Department of Nuclear Physics, Lund, Sweden.

NOTICE This document contains information of a preliminary nature and was prepared primarily for internal use at the Oak Ridge National Laboratory. It is subject to revision or correction and therefore does not represent a final report.

This report was prepared as an account of work sponsored by the United States Government. Neither the United States nor the United States Atomic Energy Commission, nor any of their employees, nor any of their contractors, subcontractors, or their employees, makes any warranty, express or implied, or assumes any legal liability or responsibility for the accuracy, completeness or usefulness of any information, apparatus, product or process disclosed, or represents that its use would not infringe privately owned rights.

I. INTRODUCTION

The use of a small Van de Graaff accelerator to generate intermediate energy neutrons has some advantages in the study of neutron interactions. The total number of neutrons produced is low, but since these can be all concentrated in a small range of energy, background effects due to unwanted neutrons can be minimized. Further improvements in background level can be achieved by:

(a) Taking advantage of the kinematics of threshold reactions such as $^{7}Li(p,n)^{7}Be$, to produce all neutrons in a narrow cone about the original direction of the proton beam;

(b) Using a pulsed beam so that the required type of events occur within a restricted interval of time, whereas the background may be largely produced by neutrons which either arrive at the detector at a different time or which have been scattered sufficiently often to arrive at the detector uniformly distributed in time.

These techniques have been applied to the study of gamma ray spectra following the capture of neutrons with energies from 5 to 100 keV. In this range, capture cross sections are less than 1 barn and often only a few millibarns. Since detectors suitable for measurement of gamma ray energies are quite sensitive to neutrons, it is only possible to observe gamma ray spectra under optimum conditions.

During 1960, two experiments were carried out, demonstrating the feasibility of such measurements. Bergqvist and Starfelt[1] used a 5 in.

LOCKHEED MARTIN ENERGY RESEARCH LIBRARIES
3 4456 0514451 8

by 4 in. NaI detector in a ring geometry experiment to measure the general shape of the gamma ray spectra from a number of elements for neutrons from 10 to 300 keV. Firk and Gibbons[2] used a larger NaI detector (9 in. x 6 in.) at 90° to the direction of the proton and neutron beams and were able to observe some of the features of the shape of gamma ray spectra for capture of 30 ± 10 keV neutrons. This work showed that by shielding the detector it was possible to remove nearly all prompt scattered neutrons.

Bird, Gibbons and Good[3] used a very similar arrangement, but with a better quality detector to study gamma ray spectra in more detail. In particular, the detector was 9 in. by 12 in. NaI and it was well shielded. Being more effectively screened from prompt neutrons, this detector could be stationed at longer flight paths and on account of the time-of-flight energy determination, more detailed results as a function of neutron energy could be obtained accordingly. Some of the results of these measurements have been published[3-9] and additional measurements using the same equipment have been made by Bergqvist, Biggerstaff, Gibbons and Good[10-12].

The purpose of this report is to present a summary of essentially all the data obtained at ORNL with the 9 in. x 12 in. NaI Spectrometer used with the pulsed 3 MeV Van de Graaff. In all, 36 elemental or separated isotopic targets were studied under experimental conditions which were continually improved during the course of the work. Although some of the data have previously been presented and discussed[3-12] many of the spectra and some of the intensity information have not been published. No distinction has been made in regard to prior publication so

far as inclusion in this report is concerned. The full set of spectra and analyzed intensities that were obtained are presented. For the reasons just stated, however, there does exist a general lack of uniformity in preparation and presentation, which however seems tolerable on the basis that much of the work presented has not since been duplicated, and the data as they are given herein provide the only available information on gamma ray spectra for the capture of 10-100 keV neutrons.

The advent of Ge(Li) detectors with their superior energy resolution has made possible great improvements in the spectra as obtained with NaI and presented here. A number of chopper and linear accelerator facilities are already using Ge(Li) detectors to study resonances below 10 keV, and with improvements in techniques these will presumably be extended to higher neutron energies. Meanwhile, Allen, Bird and Kenny[13] have developed methods for using a Ge(Li) detector in association with a Van de Graaff neutron source. This work will supersede the NaI results for cases in which sufficient target material is available to offset the low efficiency of Ge(Li) detectors.

II. METHODS

The experimental arrangement used in this work is shown in Figure 1. The ORNL 3 MV Van de Graaff provides a pulsed proton beam with a pulse width of 4 ns or better and repetition rate of 1 MHz. This beam strikes a spray-cooled thin lithium target after passing through a beam pickoff which gives an output pulse defining the time of arrival of the proton pulse. For most of the measurements, the proton energy had a value between 5 and 15 keV above the threshold for the $^{7}Li(p,n)^{7}Be$ reaction. At

5 keV the half angle of the neutron cone is approximately 20° and neutrons are produced in the energy range from 10 to 60 keV. Higher proton energies were used for studying resonances at neutron energies up to 120 keV. Flight paths from 13 to 63 cm were used depending on the amount of target material available and the capture cross section. Neutron capture targets were from 2 in. to 7 in. in diameter and had various thicknesses. In some cases dish-shaped targets (with radius of curvature equal to flight path length) were used for best neutron energy resolution. Typical values of experimental parameters are listed in Table I, but for many target materials several sets of measurements were made with different experimental conditions.

II.1 ELECTRONICS

The detector output pulses which defined the time of neutron capture were stored according to pulse height and subsequently analyzed to obtain gamma ray energy. Cross-over timing yielded an overall time resolution of 15 ns (FWHM) for a decade range of pulse heights. Both the detector output pulse and the output of a time-amplitude converter were fed to a three parameter analyzer having 2048 storage locations. A stacked discriminator type of 20 channel analyzer was used to analyze one pulse and provide gating signals to subdivide the main store into 128 channel segments. When required, gating pulses could be paralleled in groups and 256 or 512 channel segments used in the main store. Although this system lacked sufficient channels for a complete analysis of both time and amplitude, it allowed considerable flexibility for studying the most important features of both parameters.

II.2 DETECTOR AND SHIELDING

The detector mentioned earlier, was a 9 in. diameter and 12 in. long sodium iodide crystal with seven 3 in. photomultipliers connected in parallel. The pulse height resolution for ^{137}Cs gamma r ys was a little better than 10%. However, in practice, in a heavily shielded arrangement, the effective resolution was not quite so good. Figure 2 shows typical values of resolution at various gamma ray energies. It also shows the correction factor to be applied to observed pulse height peaks to obtain relative values of gamma ray intensity. The most important contribution to this correction factor is the ratio of peak height to the total area of a spectrum for one gamma ray. This changes almost linearly with gamma ray energy. In addition, the attenuation of gamma rays in the neutron shielding (see Figure 1) changes from approximately 10% at 10 MeV to 20% at 4 MeV and increases more rapidly at lower energies. The effect of attenuation of gamma rays in the neutron capture target was generally small, and has been neglected in most cases. The probability of interaction in such a large detector varies by only 2% for gamma rays up to 10 MeV.

The detector was mounted in a 4 in. thick lead shield which was lined, inside and out, with paraffin wax containing lithium or boron. At the front of the detector, an 8 in. diameter aperture in the lead shield was used in low count rate experiments, but this was reduced to 4 in. when adequate count rate was available. This aperture was covered by a 4 in. thick ^{6}Li hydride shield to minimize the transmission to the detector of scattered neutrons. The front face of the shield was aligned along a radius drawn from the neutron source at an angle of 15° or more

from the center of the neutron beam cone. The best value of signal to background ratio was obtained when the proton energy was chosen so that the neutron beam cone did not strike the detector shield. Measurements with neutrons with energies above 60 keV were affected by a rapidly rising background caused by the increase in neutron beam angle, and from the reduced effectiveness of the neutron shielding. The distance of the detector from the center of the neutron capture target was approximately 30 cm so that the solid angle was 0.7% or 2.8% of 4π depending on the size of aperture used.

A typical background spectrum is shown in Figure 3. Peaks arise from the capture of neutrons in the shield materials (Pb and H) and the detector. Other peaks in the background are from natural radioactivity, not associated with the neutron beam. The neutron separation energy in ^{128}I is 6.83 MeV and that in ^{24}Na is 6.96 MeV. Although few gamma rays of these energies appear in neutron capture spectra for sodium and iodine, summing in the large detector and the mixture of the two unresolved energies leads to the appearance of a prominent peak near 6.86 MeV. In most measurements the background shape was independent of the time after the neutron pulse, but in some cases a time dependent normalizing factor was required to give correct background estimation. The presence of the peak at 6.86 MeV makes spectral measurements more difficult at this energy but it can provide a very sensitive indicator of the amount of background which must be subtracted.

II.3 RESPONSE FUNCTIONS

The response of the detector to monoenergetic gamma rays of various energies was studied using radioactive sources and proton induced nuclear

reactions (Table II). The latter were studied with the same experimental configuration as for the neutron capture measurements, by lengthening the accelerator beam tube so that appropriate targets could be mounted at the position normally occupied by the neutron capture target. The results were corrected by subtraction of small contributions from cascade gamma rays so that a response function was obtained at each gamma ray energy.

The response functions are shown in Figure 4 and 5 for 8 in. and 4 in. collimation respectively. Backscattering and other effects which give rise to an increase in counts for low pulse heights have been ignored and the response functions were assumed to continue horizontally to zero pulse height. Errors in this assumption should be small for the gamma ray energies of interest -2 to 10 MeV. The effect of collimation on a response function is illustrated in Figure 6. The 4 in. collimator's response function shows a marked improvement compared to that for 8 in. collimation and the peak count rate is reduced by less than the factor of four which would be expected from solid angle considerations. However, further reduction in collimator size introduces a higher proportion of scattered gamma rays, increasing the peak widths and the low energy tail.

The response functions can be fitted by the sum of two gaussians (full energy and single escape peaks) and a terminated polynomial of the form shown in the equation:

$$y_j = a_1 \exp\left\{\frac{-(x_j - x_1)^2}{2\sigma_1^2}\right\} + a_2 \exp\left\{\frac{-(x_j - x_2)^2}{2\sigma_2^2}\right\} + f(x_j) \qquad (1)$$

where $f(x_j) = (C_o + C_1 x_j^2 + C_2 x_j^4 + C_3 x_j^6) \left\{(1 - \exp C_4(x_j - x_3)\right\}^2$

for $x_j < x_3$

$= 0$ for $x_j \geq x_3$

y_j is the number of counts occurring in the pulse height interval x_j; a, C, σ and x with numerical subscripts are constants.

An example of the fit of this function to an experimental response function is shown in Figure 7. The relative heights of the peaks, the valley between peaks, and the low energy tail are smooth functions of gamma ray energy and are shown in Figure 8. By the use of families of curves of this type, or of curves giving the dependence of the constants in equation (1) on gamma ray energy, it is possible to interpolate between the energies at which the response functions were measured and produce a matrix for use in analyzing experimental spectra.

II.4 DATA ANALYSIS

The requirements for data processing vary with the mode in which measurements were made. This is best illustrated by considering typical time spectra (Figure 9). These spectra were measured using the 20 channel analyzer for gamma ray pulse height analysis. Each segment of the main store then receives a time spectrum for a predetermined range of gamma ray energies. Such results show details of the neutron energy spectra which may reveal individual resonances, as in the case of lead, or a smooth capture cross section, as in the case of cadmium. The time dependent background in these results was determined by measurements using no target or a carbon target which scatters neutrons without

observable capture. Only a small number of measurements of this type were made since, for most target materials, more channels were needed to observe structure in the gamma ray spectra.

The use of the 20 channel analyzer for time analysis leads to the accumulation of gamma ray spectra for predetermined time intervals. One such time interval was always chosen to fall in the flat part of the time spectrum corresponding to background events. The spectra were recorded on paper tape for transfer to a computer for background subtraction. The amount of background subtracted was determined from the shape of the time spectrum, and from inspection of the iodine capture peak.

Analysis of corrected spectra to obtain gamma ray intensities has been carried out by hand or computer assisted spectrum stripping or by least squares methods. A least squares fitting program* provides two methods of operation:

(a) Linear Analysis: A selected set of response functions, having positions fixed by consideration of gamma ray energies expected for a particular target, is used to obtain an estimate of peak heights for each gamma ray.

(b) Non Linear Search Analysis: Estimates are made of peak height and position for a selected set of response functions. Small shifts in peak positions are generated using response function derivatives calculated from the complete matrix of response functions. A search routine carries out repeated least squares fits as peak positions are changed and stops when a minimum is reached in the sum of squared residuals.

*Prepared by C. W. Nestor, ORNL Mathematics Panel.

Relative gamma ray intensities were obtained by application of the correction factor described earlier. Normalization to gamma rays per 100 captures requires a further assumption as to the percentage of primary gamma rays observed in each measurement. This percentage was usually taken to be the same as for the corresponding energy range in thermal capture spectra. Gamma ray energies were calculated using radioactive source calibrations and assumed energies for a small number of prominent gamma rays (e.g. ground state transition and the iodine capture peak) observed in each measurement.

III. RESULTS

Background corrected pulse height spectra are presented in Figures 10-39. Since these figures contain original representations of the data, produced at quite different times, they differ considerably in format. However, whenever possible the following information has been generally supplied: the capturing target element or isotope is used to identify the capturing reaction; the energies of expected gamma ray peaks are correlated with levels in the product nuclei; spectra at resolved neutron resonances are labeled according to the resonant energy and spectra obtained over arbitrary neutron energy intervals are labeled accordingly. The variety of neutron energy ranges that appear results from differences in the bombarding proton energy that were used and from the omission of some neutron energies when the background contribution was relatively high. However, because of the relatively poor neutron energy resolution used in many of the measurements, the range shown is only an approximate indication of the neutron energies involved.

Many neutron time of flight spectra are given as insets and the labels for individual gamma ray spectra then refer to the corresponding neutron time of flight channel number. In a few cases neutron spectra are given for particular gamma ray energies (E_γ). For Ni, Zn and Ge the inset neutron spectra were obtained by dividing the observed yield for a particular gamma ray energy, by the yield from an indium target. This removes the effects of variation of neutron number with energy, but does not include the change in capture cross section of indium. The neutron spectra for Ti, Fe and Pb have been further corrected using the indium capture cross section so that the results show relative partial capture cross sections (neglecting any "thick" target effects).

Gamma ray intensities derived from the observed spectra are listed in Tables III to XV. For the nuclei with simple level schemes it is reasonable to assume that all primary transitions have been observed and the intensities can readily be expressed as "gammas per 100 captures". For the more complex nuclei an approximate normalization has been made by assuming that the analyzed intensities add to have the same sum as is observed for thermal neutron capture. In such cases the normalization factor is given at the foot of the table. Representative results from the compilation by Bartholomew et al[17] for thermal capture are included in the tables for comparison.

REFERENCES

1. I. Bergqvist, N. Starfelt, Nucl. Phys. 22, 513 (1961); 39, 353 and 529 (1962); Arkiv for Fysik 23, 417, 425, 435 (1962).

2. F. W. K. Firk, J. H. Gibbons, Proc. Symp. on Neutron Time of Flight Methods, Saclay (1961) p. 213.

3. J. R. Bird, J. H. Gibbons, W. M. Good, Phys. Letters 1, 262 (1962).

4. J. R. Bird, J. H. Gibbons, W. M. Good, Proc. Conf. on Direct Interactions, Padua (1962) p. 305.

5. J. R. Bird, J. A. Biggerstaff, J. H. Gibbons, W. M. Good, Phys. Rev. 138, B20 (1965).

6. J. A. Biggerstaff, J. R. Bird, J. H. Gibbons, W. M. Good, Phys. Rev. 154, 1136 (1967).

7. G. J. Broomhall, J. R. Bird, Nucl. Phys. A121, 329 (1968).

8. J. R. Bird, Nucl. Phys. A120, 113 (1968).

9. B. J. Allen, Nucl. Sci. and Applications 3, 64 (1967).

10. I. Bergqvist, J. A. Biggerstaff, J. H. Gibbons, W. M. Good, Phys. Letters 18, 323 (1965).

11. I. Bergqvist, J. A. Biggerstaff, J. H. Gibbons, W. M. Good, Phys. Rev. 158, 1049 (1967).

12. I. Bergqvist, Nucl. Phys. 74, 15 (1965).

13. B. J. Allen, J. R. Bird, M. J. Kenny, AAEC/E200; Phys. Letters 27B, 638 (1968); Proc. Symp. on Neutron Capture Gamma Ray Spectroscopy, Studsvik (1969) p. 587.

14. D. Chan, "Analysis of Calcium Results", to be published.

15. G. J. Broomhall, "Analysis of Titanium Results", to be published.

16. Analysis by T. Hart.

17. G. A. Bartholomew et al, Nucl. Data A3, 367 (1967); A5, 1 (1968); A5, 243 (1969).

18. H. E. Jackson et al, Phys. Rev. Letters 17, 656 (1966).

TABLE I

EXPERIMENTAL CONDITIONS

Target	Size	Form	Flight Path (cm)	Beam Current (μA)	Time (hrs)	ΔE_p (keV)
F	½" x 6" OD	CF_2	40	4.3	~10	12
Na	(½" - 1") x 6" OD	Metal	40	4.2	~10	12
Mg	(½" - 1") x 6" OD	Metal	40	4.1	~10	30
Al	(½" - 1") x 6" OD	Metal	40	4.1	17	30,50
S	(½" - 1") x 6" OD	Metal	40	3.2	13	5,12,36
^{35}Cl	60 g	NaCl	15	4.9	12	10
K			40	4.0	7	12
Ca	1000 g	Metal	51.5	3.8	2	10
^{40}Ca	225 g	Ca_2Co_3	13	6.2	2	5
^{42}Ca	25 g	Ca_2Co_3	13	6.2	2	5
^{44}Ca	100 g	Ca_2Co_3	13	6.2	2	5
Ti		Metal	51.5	3.8	5½	10
V		Metal	13	6.2	2½	5
Fe	0.64" x 7" OD	Metal	51.5	3.8	3	12
^{54}Fe	100 g	Metal	13	6.2	6½	5
^{56}Fe	130 g	Metal	13	6.2	2¼	5
Ni		Metal	51.5	3.8	2¼	10
^{58}Ni	62 g	NiO	15			5
^{60}Ni	250 g	Metal	15			5
^{63}Cu	57 g	Metal	15			5
Zn		Metal	51.5	3.8	3	10

TABLE I (Continued)

EXPERIMENTAL CONDITIONS

Target	Size	Form	Flight Path (cm)	Beam Current (μA)	Time (hrs)	ΔE_p (keV)
Ge		Metal	51.5	3.8	$3\frac{1}{2}$	10
^{88}Sr	62 g	$SrCo_3$	13	6.2	9	5
Y			15	4.9	$17\frac{1}{2}$	10
Zr		Metal	13	6.2	$4\frac{1}{4}$	5
^{90}Zr	54 g	ZrO_2	13	6.2	$6\frac{1}{2}$	5
^{91}Zr	54 g	ZrO_2	13	6.2	$4\frac{1}{4}$	5
^{92}Zr	$55\frac{1}{2}$ g	ZrO_2	13	6.2	5	5
^{94}Zr	53 g	ZrO_2	13	6.2	3	5
Pr			30		$3\frac{1}{2}$	5
Pb	$\frac{1}{2}$" x 7" OD	Metal	51.5	3.7	5	12
^{206}Pb	$\frac{1}{2}$" x 7" OD	Metal	51.5	3.8	4	12
^{207}Pb	200 g	Metal	65		~ 16	15
Bi		Metal	35	4.9	8	10
^{238}U	1" x 3" OD	Metal	35	4.9	8	10

TABLE II

CALIBRATION GAMMA RAYS

Reaction	Proton Energy (MeV)	Gamma Ray Energy (MeV)
$^{12}C(p,\gamma)^{13}N$	1.698	3.51
$^{15}N(p,\alpha)^{12}C$	0.898	4.44*
$^{19}F(p,\alpha)^{16}O$	0.902	6.13
$^{9}Be(p,\gamma)^{10}B$	0.992*	7.48
$^{13}C(p,\gamma)^{14}N$	1.747	9.17

*F. Ajzenberg-Selove, T. Lauritsen, Nucl. Phys. A114, 1(1968).
F. Ajzenberg-Selove, Nucl. Phys. A152, 1(1970).

TABLE III

GAMMA RAYS FROM $^{19}F(n,\gamma)^{20}F$

	keV Capture					Thermal Capture (Ref 17)	
	E_R = 27 keV (J_c^π = 2-)			(50 keV (J_c^π = 1-			
E_f	E_γ	$I_\gamma^{(5)}$	$I_\gamma^{(11)}$	$I_\gamma^{(5)}$	$I_\gamma^{(11)}$	E_γ	I_γ(%)
0	6.60				5±3	6.589	8.5
						6.018	8
0.660	5.98	4	6±2	5	9)		
0.828	(5.77)			(2)	)		
0.989	5.65			5	13) 34±3		
1.064					)	5.534	5
1.312	5.32	25	32±2	5	12)	5.28	7.5
	5.10	3				5.10	4
	(4.83)	(1)		(3)			
1.851	4.66	22	50±2	5			
1.975	4.60	25		20	42±2		
2.050						4.50	5
	4.83		4		6		
	4.15	4	(4)		4	3.95	4
	3.74	3					
	3.61			11)			
				)	13±3		
	3.52	5	4±2	10)		3.52	15
	3.11		8±1		20±2		
						3.02	< 20

TABLE III (Continued)

GAMMA RAYS FROM $^{19}F(n,\gamma)^{20}F$

E_f	keV Capture E_R = 27 keV (J_c^π = 2-)		keV Capture (50 keV(J_c^π = 1-)		Thermal Capture (Ref 17)	
	E_γ	$I_\gamma^{(5)}$ $I_\gamma^{(11)}$	$I_\gamma^{(5)}$	$I_\gamma^{(11)}$	E_γ	I_γ(%)
	2.60	5±2	7±3		2.53	23
					2.45	15
	2.1		8±3		2.08	6
	1.98	8±3	6±3		1.98	5
	1.85	15±4				
	1.35	57±2	37±3		1.36	50
	1.15	16±2	3±2			
	1.06		7±3			
	1	(4)	6±3		0.984	9
	0.84	4±2				
	0.65	~ 30	≥ 30		0.655	5
					0.584	15

TABLE IV

GAMMA RAYS FROM $^{23}Na(n,\gamma)^{24}Na$

keV Capture (Ref. 11)		Thermal Capture† (Ref 17)	
E_γ	I_γ*	E_γ	I_γ(%)
6.5	9	6.486	0.5
		6.395	20.0
5.7	10	5.617	4.6
5.2	5	5.113	0.6
		5.073	0.5
4.5	9	4.496	0.4
		4.187	1.5
		3.981	13.8
		3.878	4.9
		3.587	11.6
3.4	7	3.370	2.6

*Relative Intensities (Arbitrary Units)

†Many weaker transitions omitted.

TABLE V

GAMMA RAYS FROM $^{24}Mg(n,\gamma)^{25}Mg$

	keV Capture (Ref. 10, 11)				Thermal Capture (Ref 17)	
	E_R = 50 keV		E_R=84 keV(J_c^π =3/2-)			
E_f	E_γ	I_γ(%)	E_γ	I_γ(%)	E_γ	I_γ(%)
0	7.36	56±7	7.41	18±1	7.36	(0.14)
0.584	6.75	17±3	6.83	67±2	6.734	2.8
0.976	(5.8)	(5)			6.357	5.7
1.962			5.45	2.5±1		
2.565	4.8	5±3	4.84	12.5±1.5	4.767	(0.14)
2.803	4.6	3±2			4.330	1
	(4.2)	(4)				
	(3.8)	(4)	(3.9)	(1.4)	3.918	71
					3.552	18.6
	(3.5)	(7)			3.408	11.9
	(3.2)	(7)	(3.25)	(1.2)	3.054	16.5
	2.7	10±4	(2.8)			
			(2.5)	(2.4)	2.43	11.9
			1.98	11.1±0.9		
			1.58	3.3±0.4		
			1.38	2.4±0.4		
			0.98	5.7±0.8		

TABLE VI

GAMMA RAYS FROM $^{27}Al(n,\gamma)^{28}Al$

E_f	keV Capture (Ref. 10, 11) E_R = 35 keV		89 keV(J_c^π = 3+)		120 keV	Thermal Capture (Ref. 17)	
	E_γ	I_γ(%)	E_γ	I_γ(%)	I_γ(%)	E_γ	I_γ(%)
0 0.031	7.77	60 ± 5	7.80	15 ± 2	~ 50	7.730	24
0.973, 1.017	6.74	4 ± 2	6.81	11 ± 3		6.76	1.7
1.372	(6.4)	(5)				6.35	2.3
1.633			6.11	10 ± 2		6.13	3
2.143, 2.207			5.60	14 ± 3			
2.279	5.4	4 ± 2				5.45	(1.6)
			5.18	12 ± 3		5.140	3.9
						4.91	2.4
	4.78	4 ± 2	4.80	11 ± 3		4.730	8
						4.66	5
	(4.4)	(3)	4.30	14 ± 3		4.42	1
	4.2	3				4.260	6.1
						4.13	6
	3.9	5	(3.9)	(7)		3.88	6
	3.55	4	3.55	20 ± 4		3.600	4.5
						3.470	5.2
	3.1	4	3.1	13 ± 4		3.04	5.1
	2.9	3				2.960	8
	2.6	4 ± 2	2.65	12 ± 4		2.61	5
	2.2	(9)	2.25	26 ± 5		2.28	5.1
	(2.0)	(3)				2.12	3
	1.63	20 ± 5	1.66	30 ± 5		1.64	5.4
	1.35	6 ± 2				1.31	4.9
	0.98	12 ± 3				0.97	10

TABLE VII

GAMMA RAYS FROM $^{32}S(n,\gamma)^{33}S$

E_f	keV Capture (Ref. 10, 11) E_R=30 keV(3/2-) E_γ	I_γ(%)	E_R=111 keV($\frac{1}{2}$+) E_γ	I_γ(%)	Thermal Capture (Ref 17) E_γ	I_γ(%)
0	8.7	8 ± 2	8.71	21 ± 2	8.646	2.3
0.841	7.8	60 ± 4	7.91	19 ± 3	7.804	3.8
1.965	6.7	6 ± 2			6.678	0.7
2.313	6.4	10 ± 3				
3.224	5.5	8 ± 4	5.53	30 ± 4	5.425	5.7
	4.8	10 ± 4		~ 20	4.874	11.6
			(3.8)	(~≤ 5)	3.726	3.2
			3.40	10 ± 5	3.370	5.1
			3.22	18 ± 8	3.221	22
			3.0	10 ± 5	2.931	15
			2.38	31 ± 5	2.379	41
	0.84	90 ± 10			0.842	65

TABLE VIII

GAMMA RAYS FROM $^{35}Cl(n,\gamma)^{36}Cl$

	keV Capture (Ref. 11)			Thermal Capture† (Ref 17)	
		Relative Intensities			
E_f	E_γ	E_n 25 keV	E_n 50 keV	E_γ	I_γ(%)
0	8.60	1.0	1.0	8.582	3.1
0.788	7.78	1.2	1.2	7.794	8.2
1.163	7.44	0.6	1.4	7.419	12.7
1.600	7.00	0.2	2.0	6.982	2.7
1.950)) 1.957)	6.65	0.8	2.3	6.626	13.6
2.467	6.2	0.3	4.5	6.115	25.2
	5.9	0.4		5.906	1.3
	5.6	0.5		5.720	6.1
	5.0	0.5		4.982	4.2
	4.6	~ 0.2		4.444	1.1
	4.1	~ 0.3		4.080	0.7
	3.6	~ 0.4			
	2.9	~ 0.4			
	2.6	~ 0.2			
	1.94	~ 0.5	6.7	1.950	18.5
	1.58		3.3	1.600	3.2

†Many weaker transitions omitted.

TABLE IX

GAMMA RAYS FROM CALCIUM

$^{40}Ca(n,\gamma)^{41}Ca$				$^{42}Ca(n,\gamma)^{43}Ca$				$^{44}Ca(n,\gamma)^{45}Ca$			
		Thermal	keV (Ref 14)			Thermal	keV (Ref 14)			Thermal	keV (Ref 14)
E_f	E_γ	$I_\gamma(\%)$	I_γ^*	E_f	E_γ	$I_\gamma(\%)$	I_γ^*	E_f	E_γ	$I_\gamma(\%)$	I_γ^*
0	8.364		1	0	7.933		2	0	7.415		1
1.943	6.421	43.5	12	0.374	7.559		3	0.174	7.341		4
2.010	6.352	0.2	(<5)	0.593	7.340	5.7	3½	1.436	5.980	10.7	8
2.463	5.901	7.0	16	0.993	6.940		2	1.903	5.512	54.5	25
2.670	5.962	1.1	5	1.389	6.544		1½	2.256	5.159	9.7	8
2.961	5.403		3	1.957	5.976	0.6	3	2.847	4.568	4.1	9
3.050	5.314	0.3	2	2.043	5.885	53	8½	3.247	4.168	2.4	11
3.400	4.963	1.8	3	2.753	5.180		2	3.422	3.993	10.2	9
3.495	4.869		4	2.947	4.986	3.6	5	3.786	3.629	1.0	15
3.614	4.750	2.6	1	3.074	4.837	0.1	6	3.845	3.570	1.3	4
3.730	4.634		5	3.194	4.739		3				
3.845	4.519	0.7	4	3.293	4.640	2.4	6				
3.945	4.419	17.1	5	3.566	4.367	2.9	3				
4.187	4.177		3	3.655	4.278		2				
4.603	3.760	3.1	9	3.898	4.035		12				
4.753	3.610	6.0	5	4.196	3.727	8.3	6				
5.012	3.351	0.4	4	4.239	3.694		8				
5.082	3.282		2								

*Normalization ΣI_γ = 84%

*Normalization ΣI_γ = 76½%

*Normalization ΣI_γ = 94%

TABLE X

GAMMA RAYS FROM TITANIUM

E_f	Product Nucleus	keV Capture (Ref. 15) Relative Intensities						I_γ*	Thermal Capture (Ref 17)	
		E_γ	12keV	17keV	22keV	35keV	50keV	10-90 keV	E_γ	I_γ(%)
1.555	^{50}Ti	9.4						1.4	9.376	4.7
2.423	^{48}Ti	9.1						1	9.189	4.0
	$^{48}Ti, ^{50}Ti$	8.32						1.7	8.342	10
0	^{49}Ti	8.14				0.25		0.6		
1.376	^{49}Ti	6.74	5	4	2	3	0.6	36	6.753	43
1.583	^{49}Ti	6.55	< 0.04	0.4	$2\frac{1}{2}$	1.2	0.1	7	6.550	6.2
1.717	^{49}Ti	6.41	6	5	2	0.1	0.2	32	6.413	31

*Normalization $\Sigma I_\gamma(^{49}Ti) = 76\%$.

TABLE XI

GAMMA RAYS FROM IRON

$^{54}Fe(n,\gamma)^{55}Fe$					$^{56}Fe(n,\gamma)^{57}Fe$				
	keV Capture (Ref 8)		Thermal Capture† (Ref 17)			keV Capture (Ref 8)		Thermal Capture† (Ref 17)	
E_f	E_γ	I_γ*	E_γ	I_γ(%)	E_f	E_γ	I_γ*	E_γ	I_γ(%)
0	9.33	17	9.295	65	0,0.014	7.68	33		46
0.413	8.92	9	8.886	12	0.135	7.55	10½		
0.933	8.40	9			0.365	7.29	2½	7.277	5.6
1.322	8.04	4			0.706	6.98	5		
1.413	7.81	2			1.264	6.42	6	6.379	0.7
1.925)	7.35	9½	7.377	0.1	1.629	6.04)	6½		
2.058)			7.248	1.8	1.727	5.94)		5.920	8.9
	7.12	3½				5.54	1	5.499	0.2
2.478	6.85	7½	6.828	2.1		5.33	1		
2.940	6.43	7½				4.98	12½	4.950	0.8
	6.25	5½	6.266	3.5				4.810	2.0
	5.97	4				4.72	9½	4.680	0.4
			5.746	2.6		4.55	4	4.405	1.5
	5.54	9	5.509	2.9		4.32	6	4.217	3.5
	5.3	5	5.391	1.1		3.89	2½	3.855	1.3
	4.98	8	4.802	3.3		3.48	4½	3.440	2.4
			4.707	1.2				3.416	2.7
	4.66		4.587	2.7		3.20	5	3.272	1.8
			4.495	3.4				3.192	1.1
	4.05	7	4.180	0.8		2.93	7	2.955	0.8
	3.82	6	3.792	1.8		2.67	17½	2.720	2.3
	3.37	8	3.548	1.4		2.19	9	2.138	0.9
	2.97	17½	3.028	2.6					
	2.48	19½	2.470	3.9					
	1.97	23	2.052	2.0					
			1.918	2.1					

*Normalization ΣI_γ(> 4.7 MeV)= 100%

*Normalization ΣI_γ(> 3.8 MeV)= 100%

†Many weaker transitions omitted.

TABLE XII

GAMMA RAYS FROM Sr and Y

$^{88}Sr(n,\gamma)^{89}Sr$			$^{89}Y(n,\gamma)^{90}Y$				
	keV Capture (Ref 16)			keV Capture		Thermal Capture (Ref 17)	
E_f	E_γ	I_γ*	E_f	E_γ	I_γ*	E_γ	I_γ(%)
0	6.40	3.4	0	6.88	2	6.85	0.3
1.05	5.35	2.5	0.203	6.68	5	6.646	0.8
2.09	4.38	2.8	0.680				
			0.780	6.10	2	6.084	45
			1.045	5.9	$1\frac{1}{2}$		
			1.214	5.66	2	5.647	2
			1.374	5.49	6	5.482	

*Relative Intensities (arbitrary units).

TABLE XIII

GAMMA RAYS FROM ZIRCONIUM

$^{90}Zr(n,\gamma)^{91}Zr$				$^{91}Zr(n,\gamma)^{92}Zr$			
	keV Capture (Ref 16)		Thermal Capture (Ref 17)		keV Capture (Ref 16)		Thermal Capture (Ref 17)
E_f	E_γ	I_γ*	E_γ	E_f	E_γ	I_γ*	E_γ
0	7.17	10.6		0	8.71	1.7	8.66
0.91				0.93	7.74	5.3	7.71
1.208	5.96	9.5		1.39)			
1.40				1.50)	7.17	4.8	
1.46	5.61	2.1		1.69)			
1.87				1.84)	6.87	~ 2	
2.07)				1.90			
2.19)	5.0	2.5	4.8	2.05	6.62	3	
2.56	4.57	5	4.6	2.16			
	3.5	~ $3\frac{1}{2}$	3.5	2.27	6.31	~ 2	6.30
	2.55	~ 6					
	2.08						

$^{92}Zr(n,\gamma)^{93}Zr$				$^{94}Zr(n,\gamma)^{95}Zr$			
	keV Capture (Ref 16)		Thermal Capture (Ref 17)		keV Capture (Ref 16)		Thermal Capture (Ref 17)
E_f	E_γ	I_γ*	E_γ	E_f	E_γ	I_γ*	E_γ
0	6.74	5.2		0	6.52	2.3	6.4
0.267	6.46	5.2		0.92	5.57	3.2	6.1
0.935	5.82	4.3			4.92	2.1	
1.42	5.29	6.5	5.27		4.46	1.9	
1.64					4.25	~ 2	
1.94	4.77	~ $3\frac{1}{2}$					4.1
2.08	4.67	~ 2					3.7
2.32							3.0
2.50	4.22	~ 3	4.26				

*Relative Intensities (arbitrary units).

TABLE XIV

GAMMA RAYS FROM ^{195}Pt

E_f	Resonance Capture			Thermal Capture (Ref 17)	
	E_γ	I_γ*		E_γ	I_γ(%)
		keV[9]	eV[18]		
0	7.92	1.0	1.0	7.920	0.56
0.356	7.56	0.76	0.6	7.566	0.17
0.689	7.23	0.8	0.7	7.230	0.46
0.877					
1.015					
1.117	6.78	0.5	0.35		
1.143				6.776	0.06
1.182				6.738	0.06
1.320					
1.362	6.52	0.7	0.55	6.562	0.2
1.404				6.320	0.06
1.447					

*Relative Intensities (arbitrary units).

TABLE XV

GAMMA RAYS FROM Pb

$^{206}Pb(n,\gamma)^{207}Pb$		keV Capture ; Intensities(%) (Ref 6)					Thermal Capture (Ref 17)	
E_f	E_γ	E_R = 16.5 keV	21 keV	25 keV	35,46 keV	66,72 keV	E_γ	I_γ(%)
0	6.76	73 ± 3	≤ 4	36 ± 4	8 ± 2	48 ± 3	6.736	
0.570	6.19	≤ 6	34 ± 8	24 ± 2	15 ± 3	10 ± 3		
0.897	5.89	17 ± 3	19 ± 8	≤ 2	47 ± 3	23 ± 2		
	4.15	≤ 4	10 ± 5	26 ± 5	15 ± 3	7 ± 7		
	3.55	10 ± 5	36 ± 12	14 ± 10	15 ± 8	12 ± 7		

$^{207}Pb(n,\gamma)^{208}Pb$		keV Capture (Ref.(6,7)) ; Intensities (%)				Thermal Capture (Ref 17)	
E_f	E_γ	E_R = 17 keV	22 keV	30 keV	42 keV	E_γ	I_γ(%)
0	7.41	30		80	95	7.368	100
2.614	4.79	70		20	5		
	2.61	50		20	3		
		Relative Resonance Areas					
0	7.41	0.15	≤ 0.1	0.2	1.0		

TABLE CAPTIONS

Table I	Experimental Conditions
Table II	Calibration Gamma Rays
Table III	Gamma Rays from $^{19}F(n,\gamma)^{20}F$
Table IV	Gamma Rays from $^{23}Na(n,\gamma)^{24}Na$
Table V	Gamma Rays from $^{24}Mg(n,\gamma)^{25}Mg$
Table VI	Gamma Rays from $^{27}Al(n,\gamma)^{28}Al$
Table VII	Gamma Rays from $^{32}S(n,\gamma)^{33}S$
Table VIII	Gamma Rays from $^{35}Cl(n,\gamma)^{36}Cl$
Table IX	Gamma Rays from Ca
Table X	Gamma Rays from Ti
Table XI	Gamma Rays from Fe
Table XII	Gamma Rays from Sr and Y
Table XIII	Gamma Rays from Zr
Table XIV	Gamma Rays from ^{195}Pt
Table XV	Gamma Rays from Pb

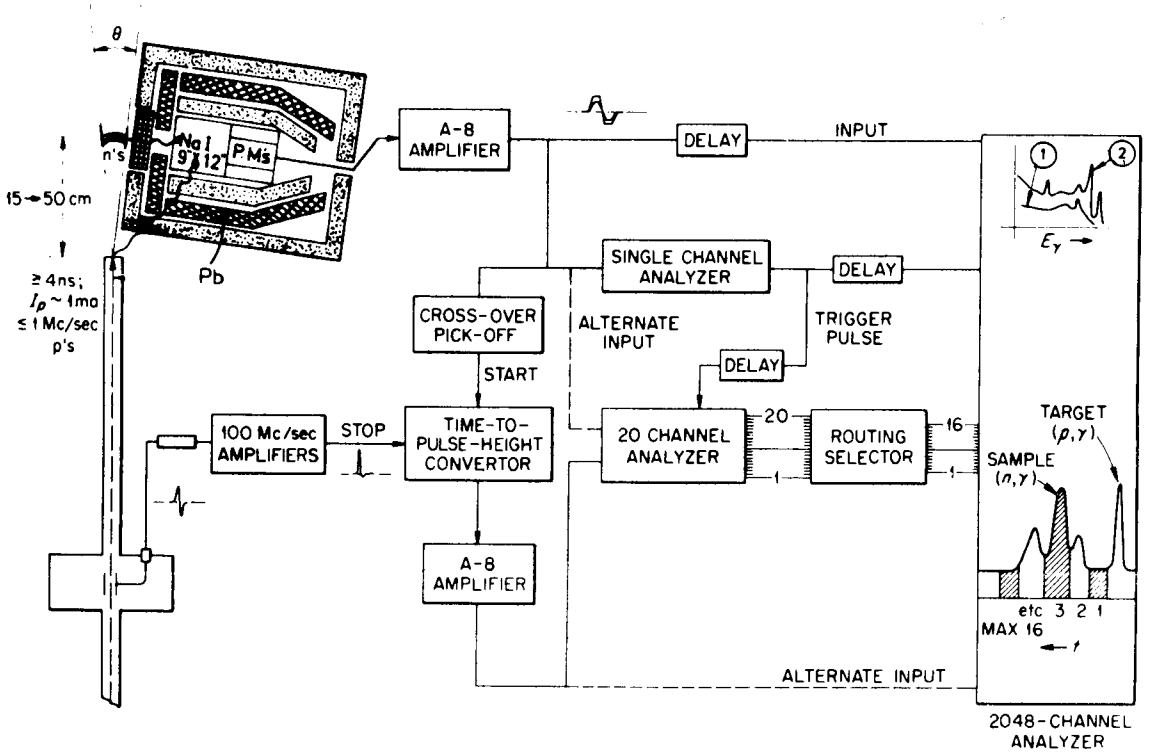

Figure 1 Equipment for measurement of neutron time of flight and gamma ray energy for keV neutron capture.

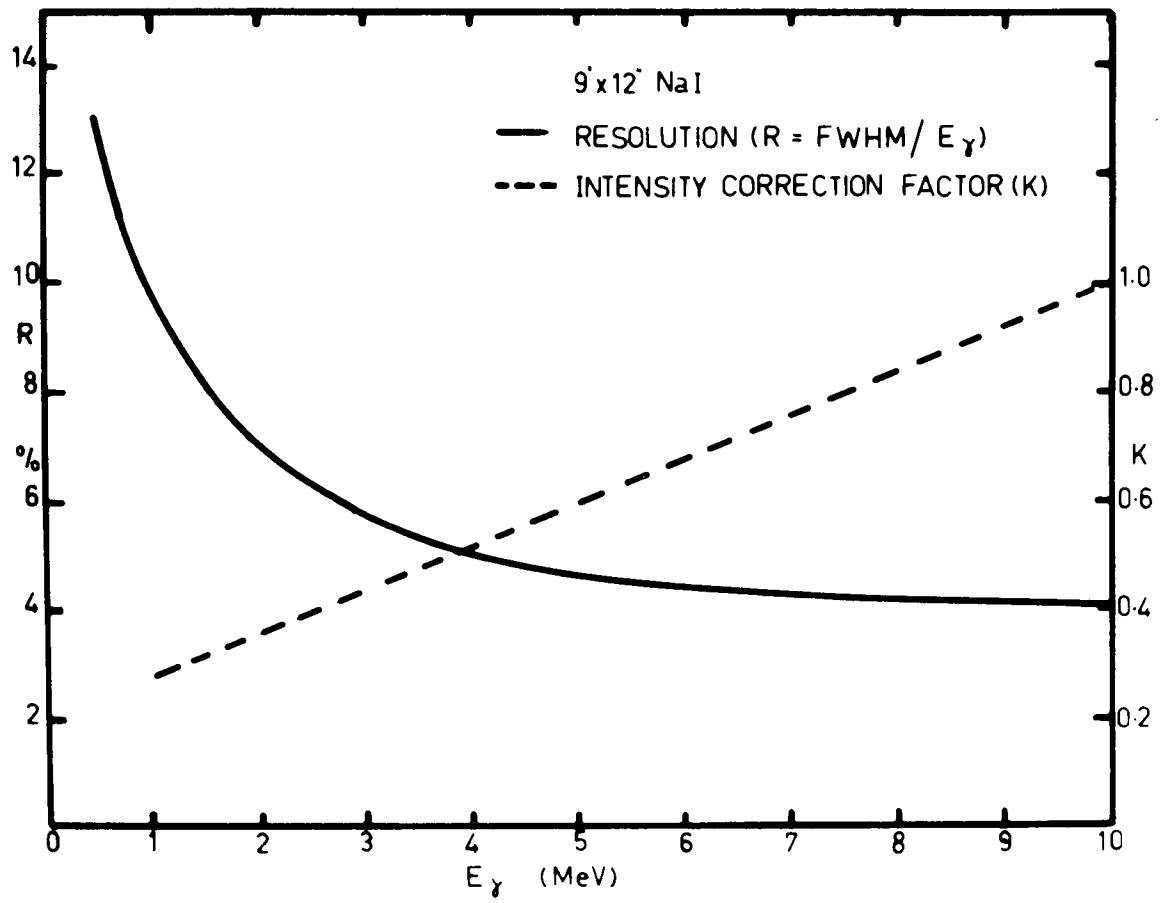

Figure 2 Resolution (R) and intensity correction factor (K) as a function of gamma ray energy (E_γ).

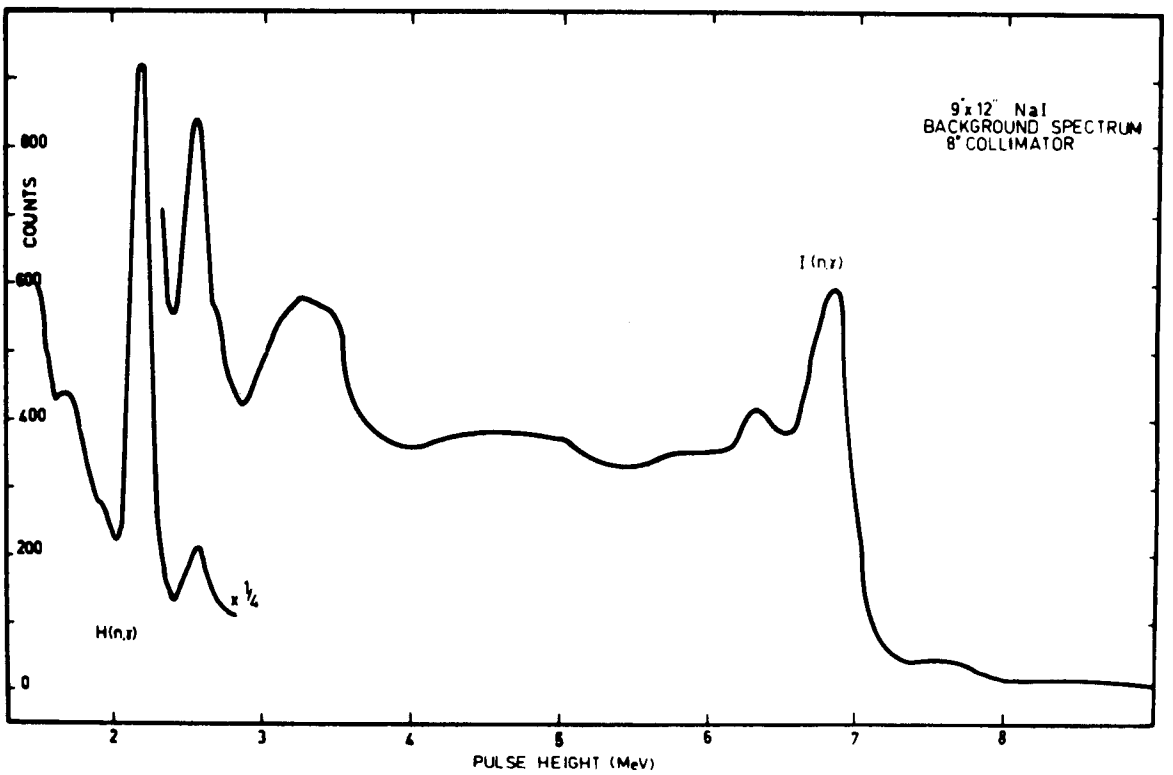

Figure 3 Typical background pulse height spectrum.

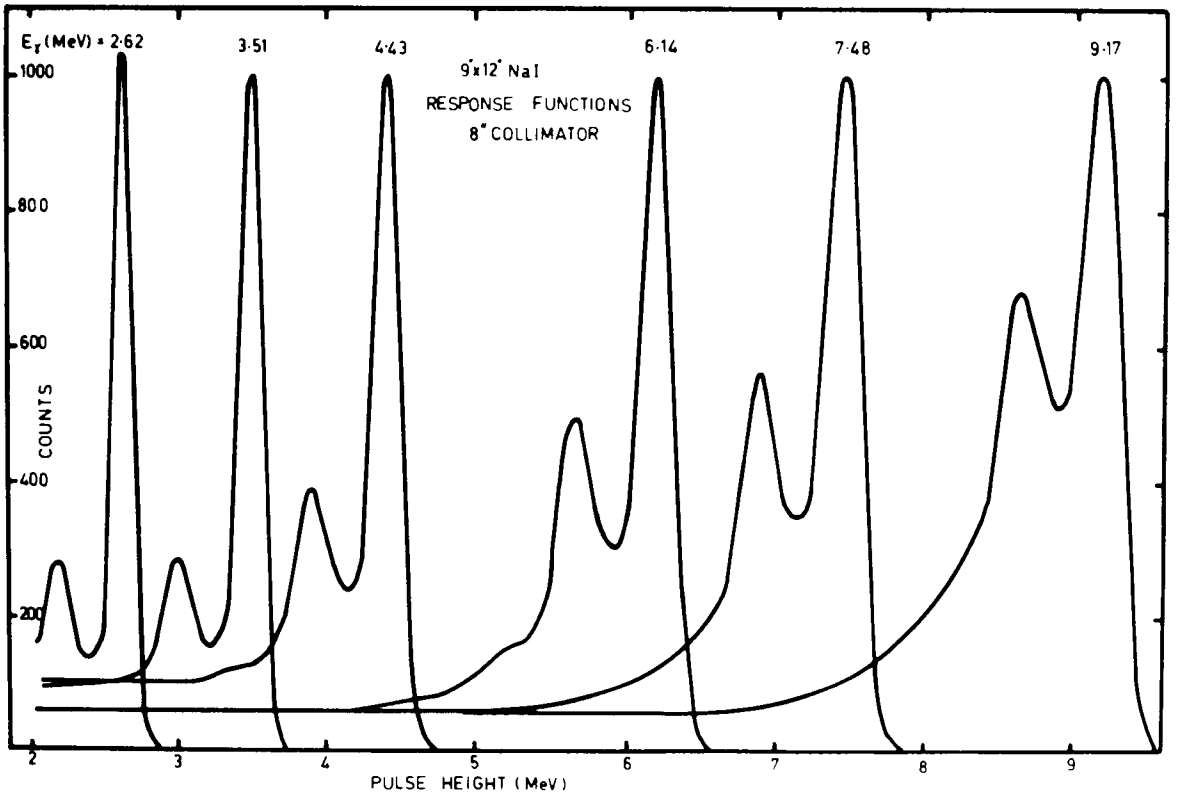

Figure 4 Detector response functions using an 8" collimator.

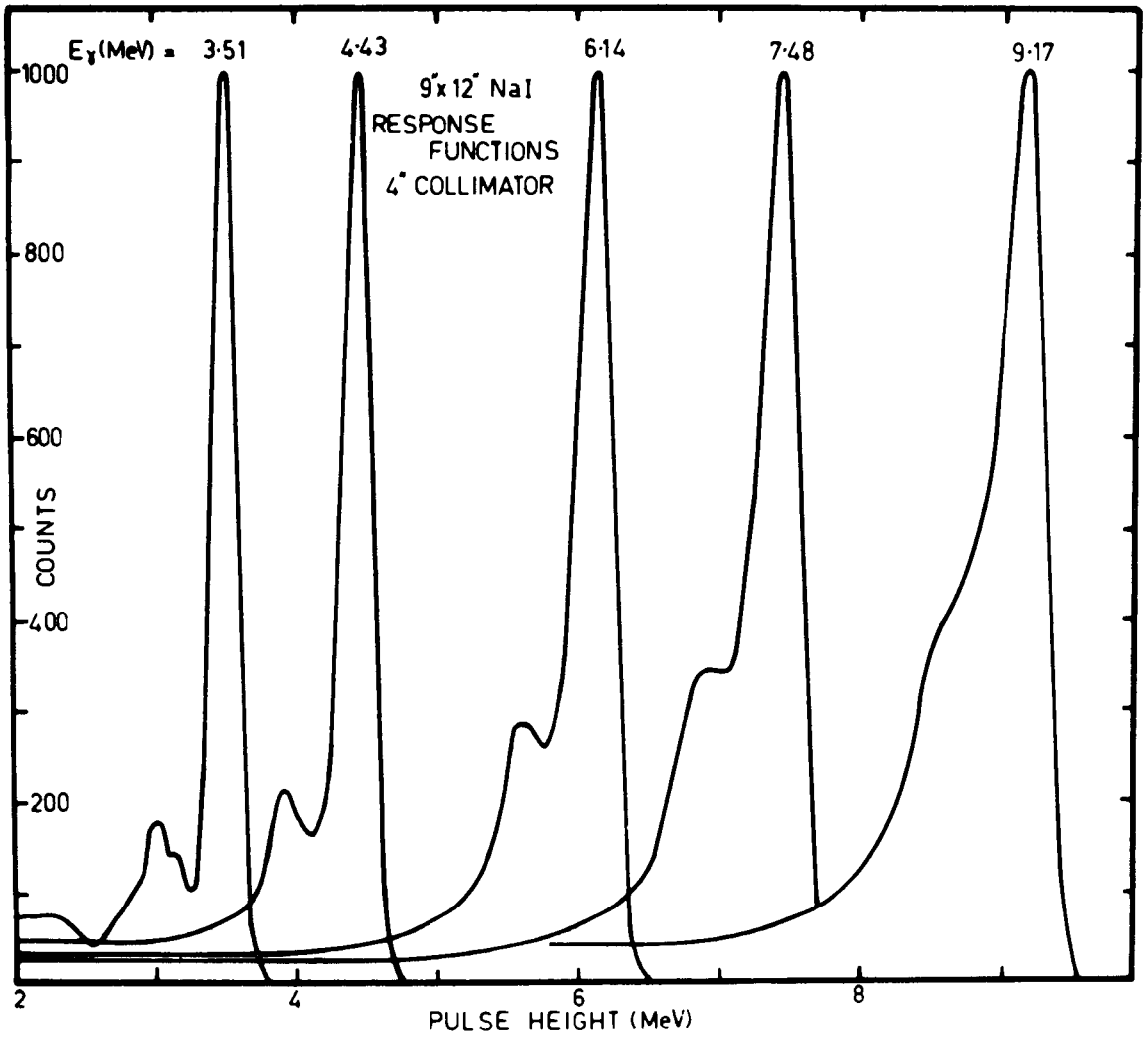

Figure 5 Detector response functions using a 4" collimator.

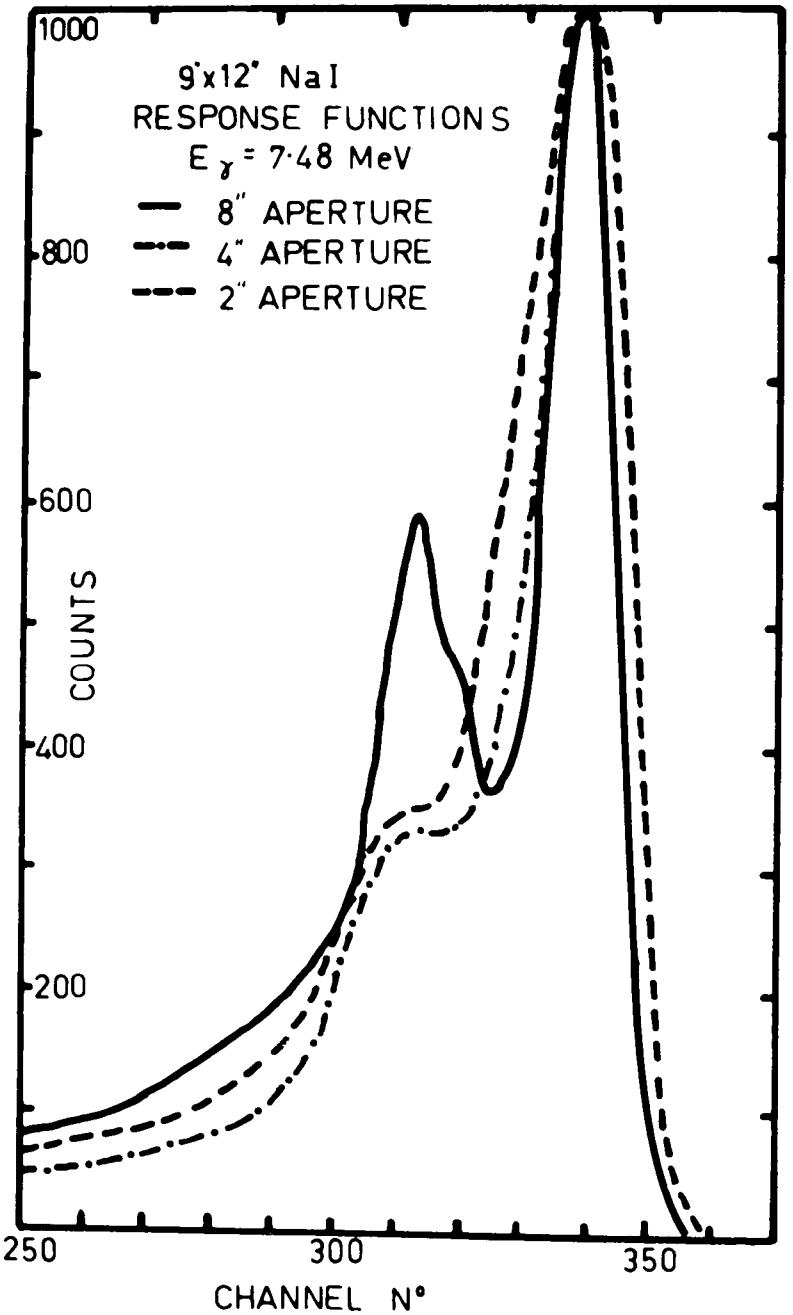

Figure 6 Effect of collimating aperture on response function at 7.48 MeV.

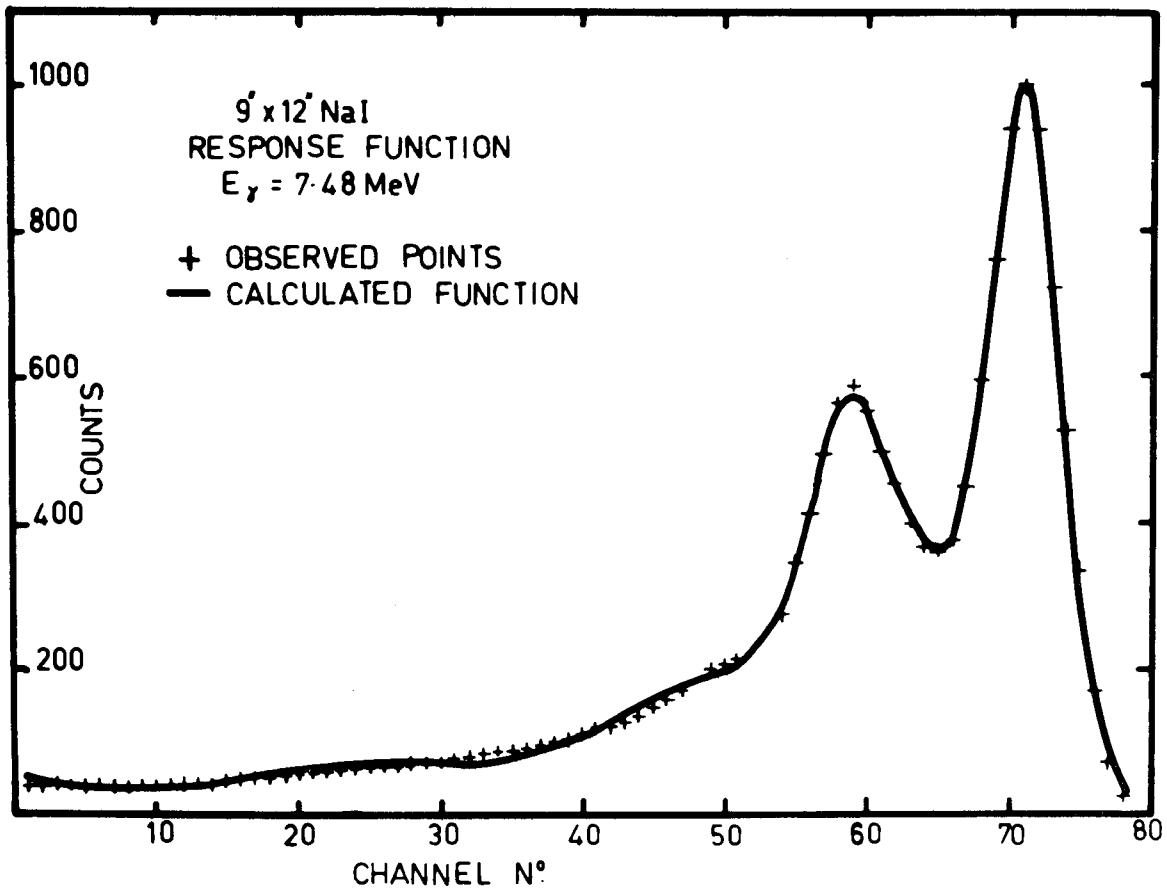

Figure 7 Comparison of 7.48 MeV response function and calculation using equation (1).

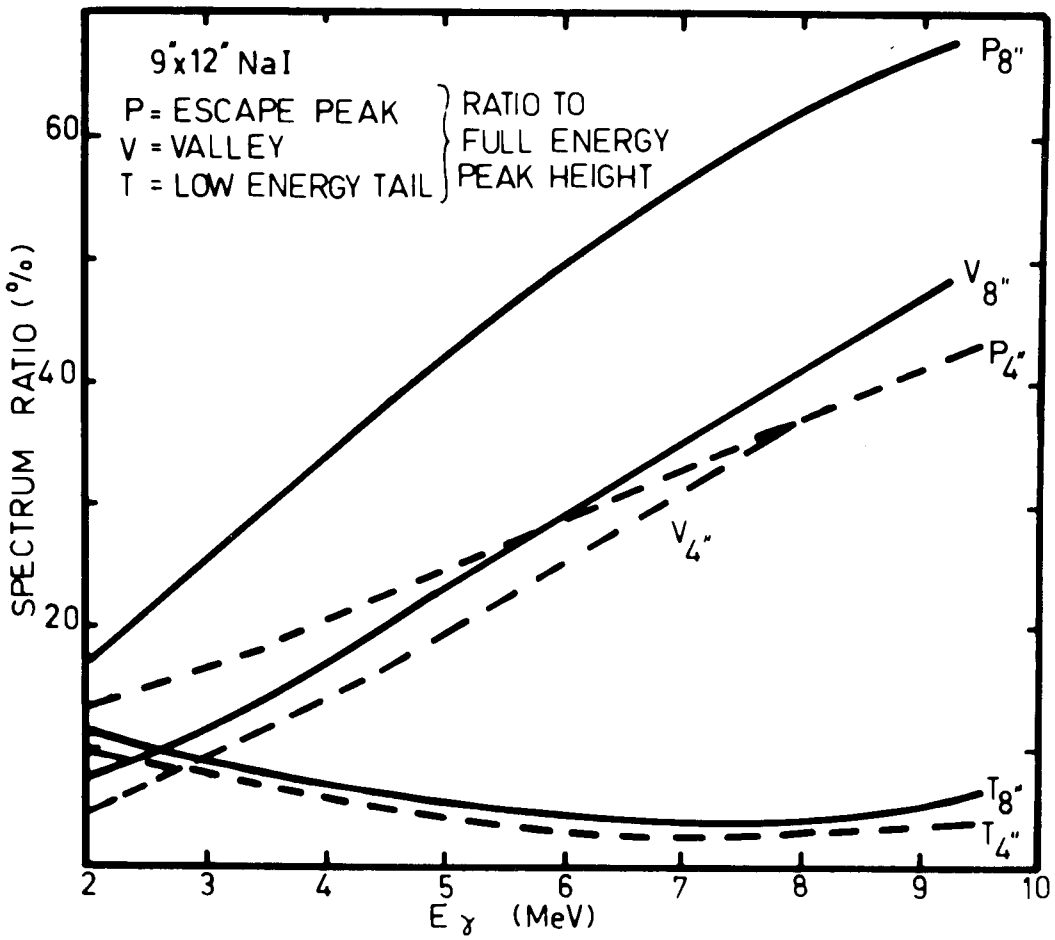

Figure 8 Variation of pulse height spectrum ratios with gamma ray energy.

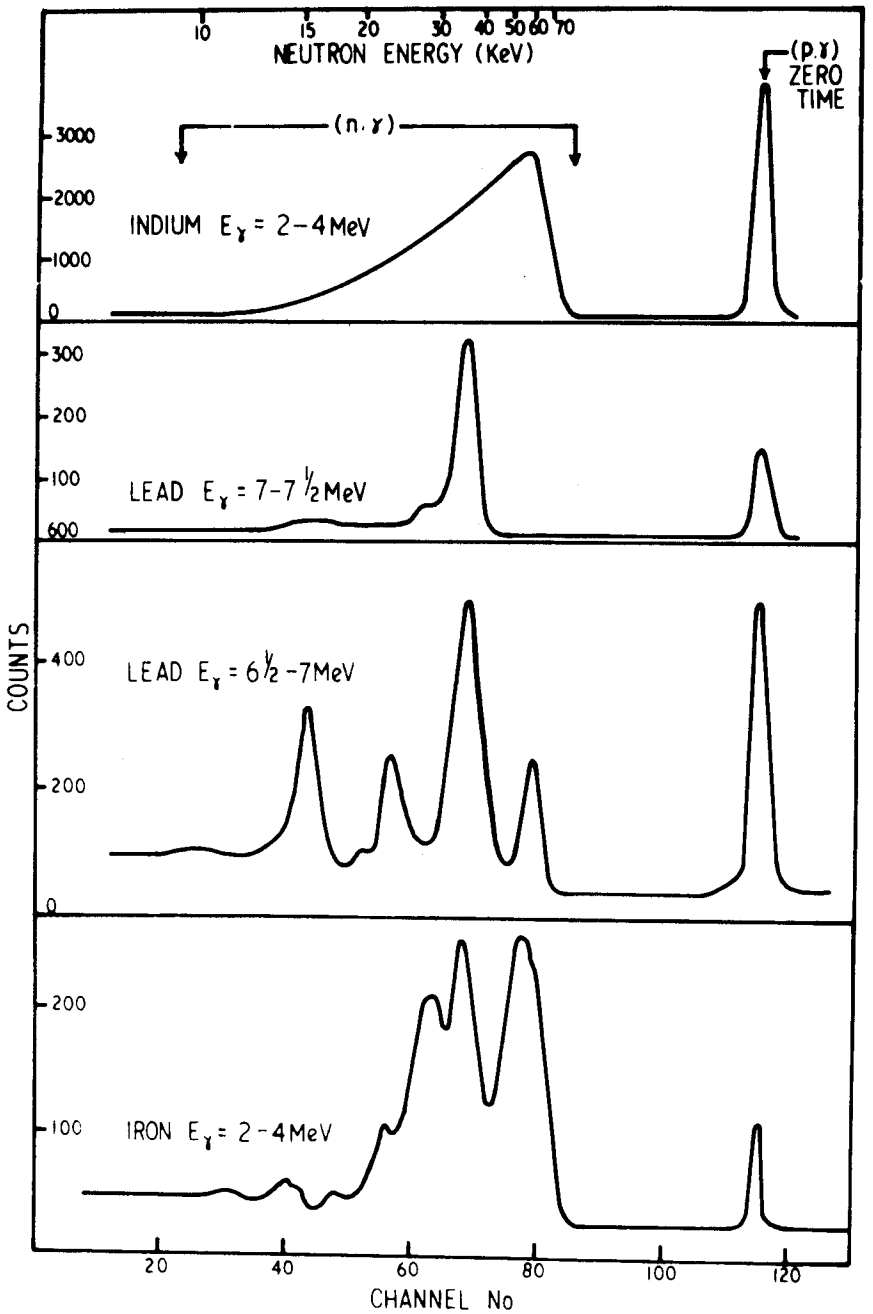

Figure 9 Typical neutron time of flight spectra for $E_\gamma > 3$ MeV using a 51 cm flight path.

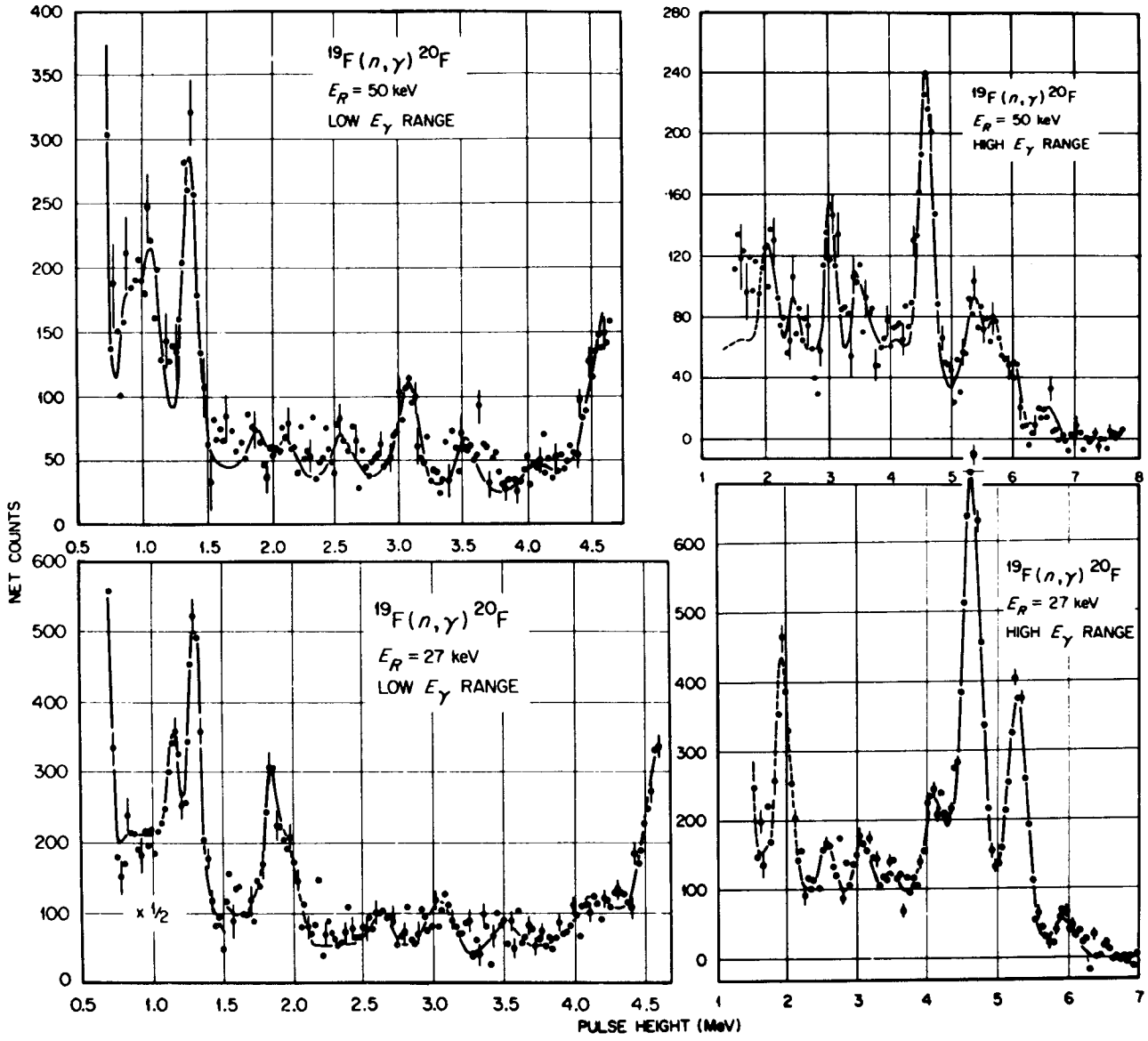

Figure 10 Gamma ray spectra for resonances at 27 keV and 50 keV in ^{19}F (Ref. 11).

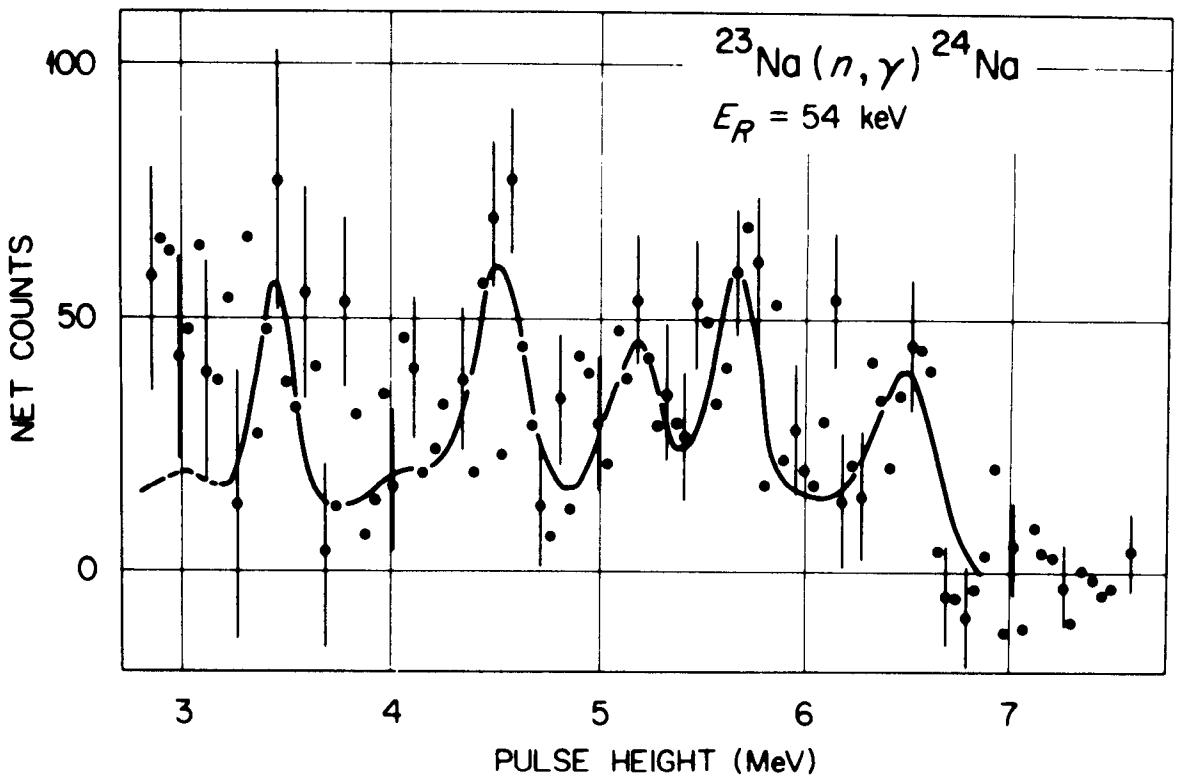

Figure 11 Gamma ray spectrum for the 54 keV resonance in sodium.

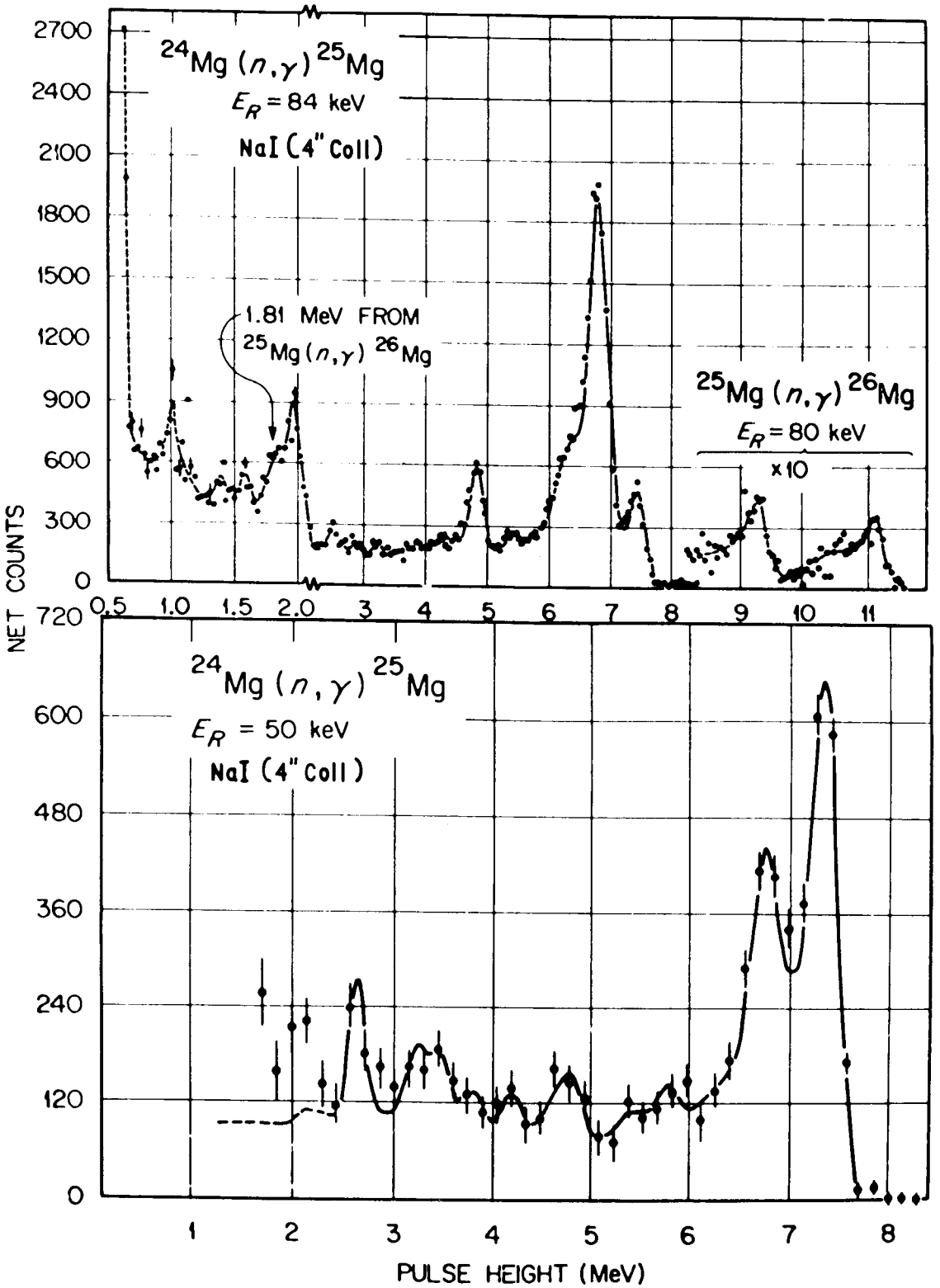

Figure 12 Gamma ray spectra for resonances in ^{24}Mg and ^{25}Mg (Refs. 10,11).

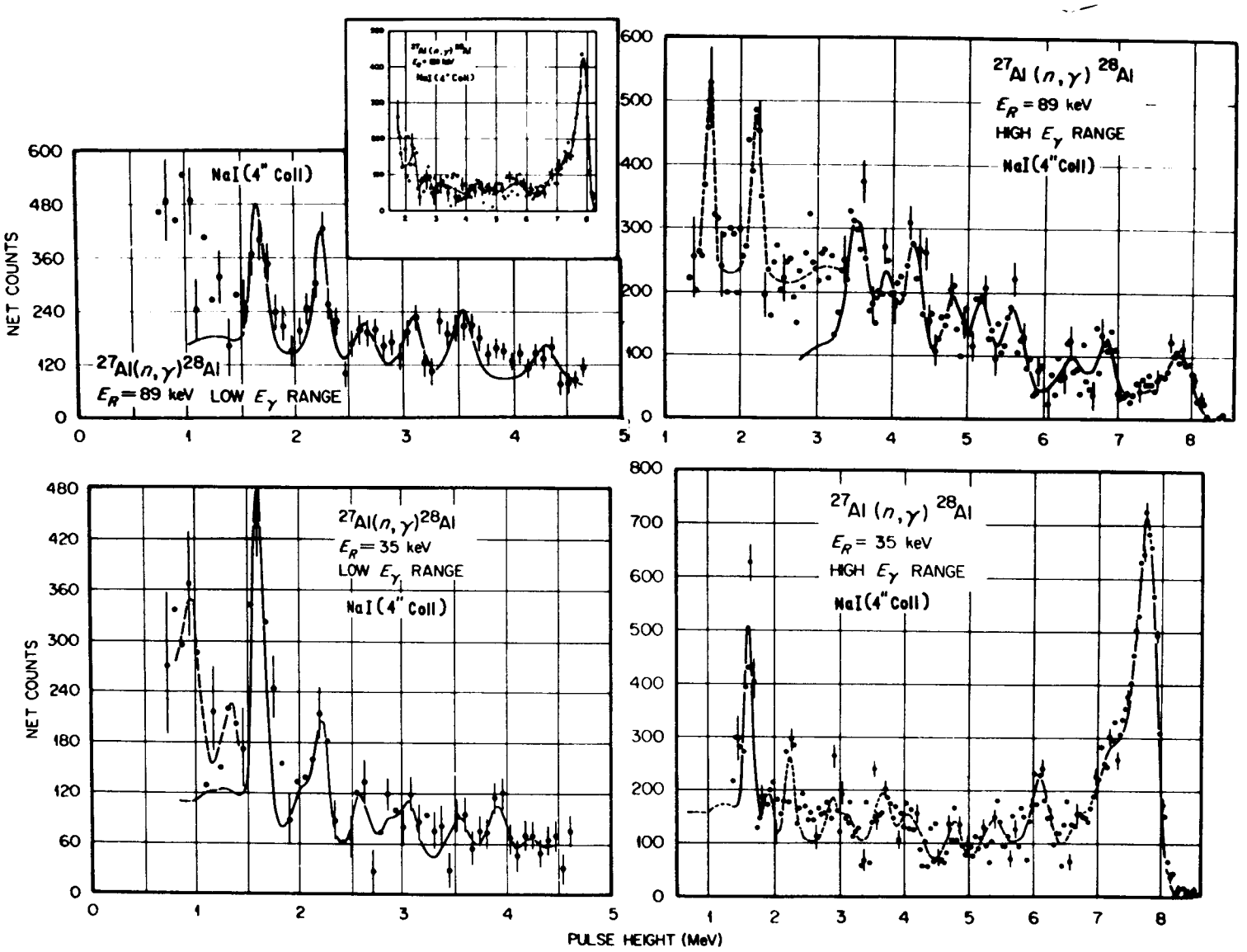

Figure 13 Gamma ray spectra for resonances at 35 keV, 89 keV and 120 keV in ^{27}Al (Refs. 10, 11).

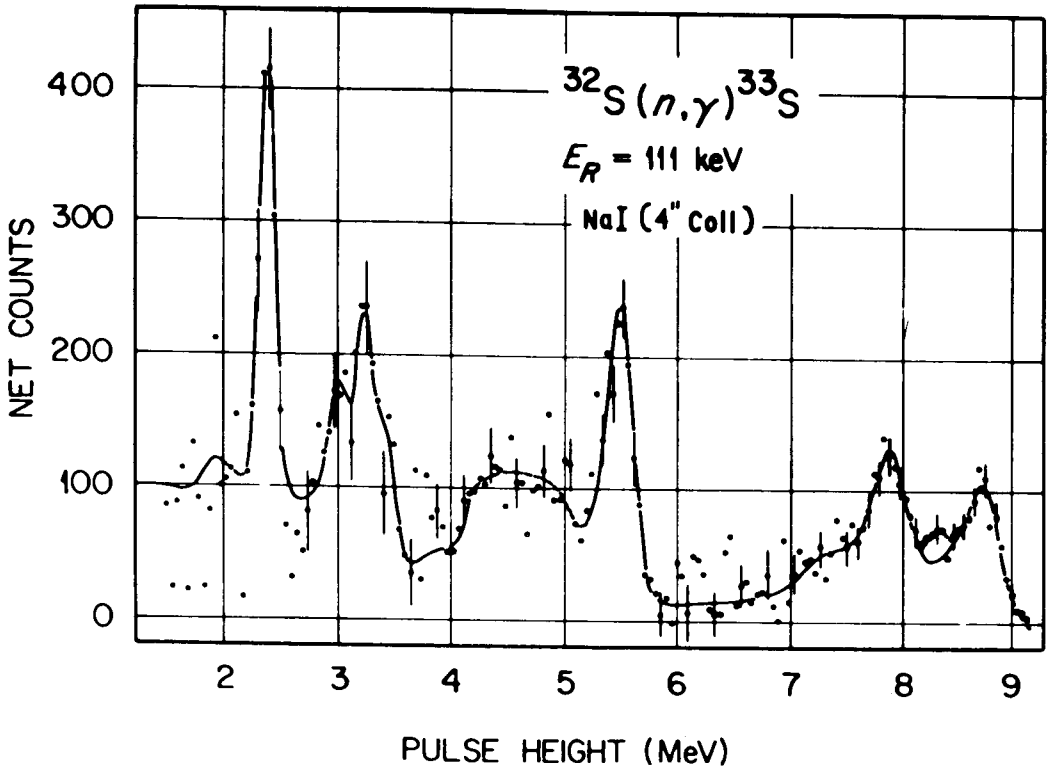

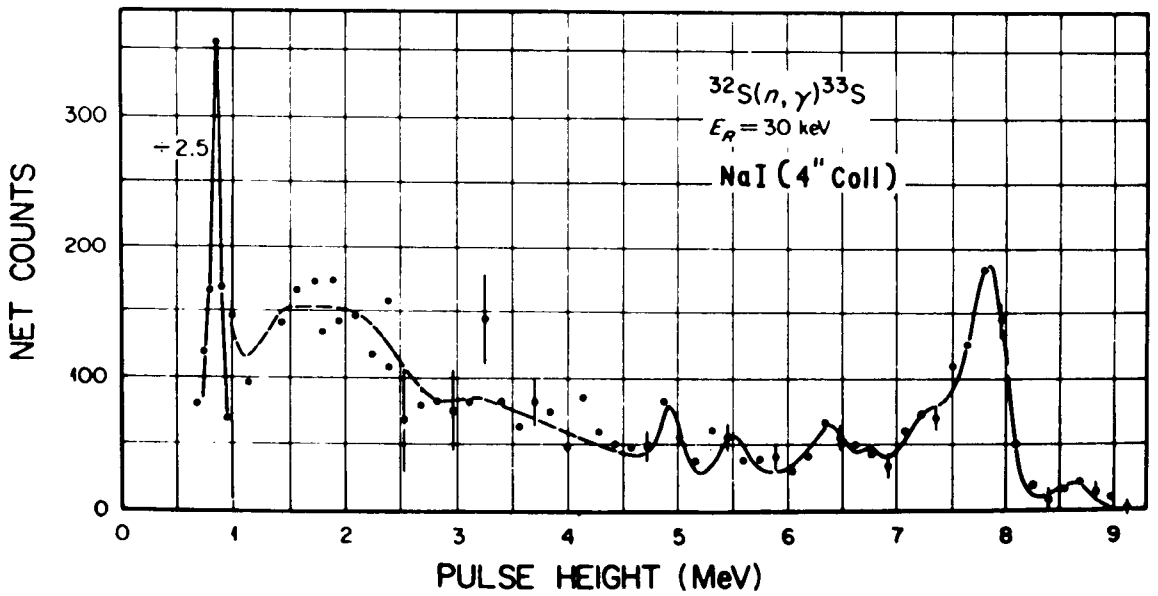

Figure 14 Gamma ray spectra for resonances at 30 keV and 111 keV in ^{32}S (Refs. 10, 11).

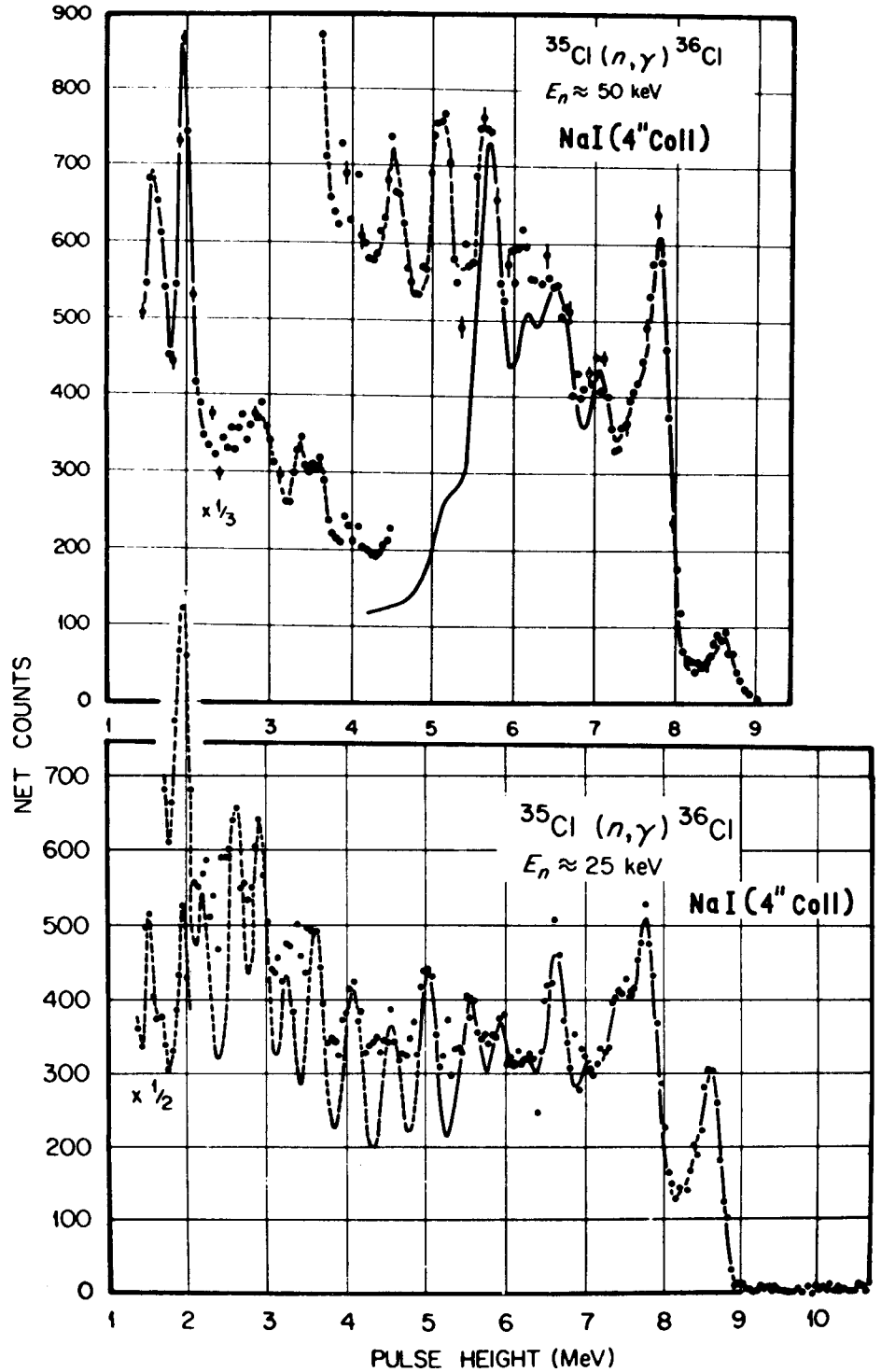

Figure 15 Gamma ray spectra for neutron energies of 25 keV and 50 keV in ^{35}Cl (Ref. 11).

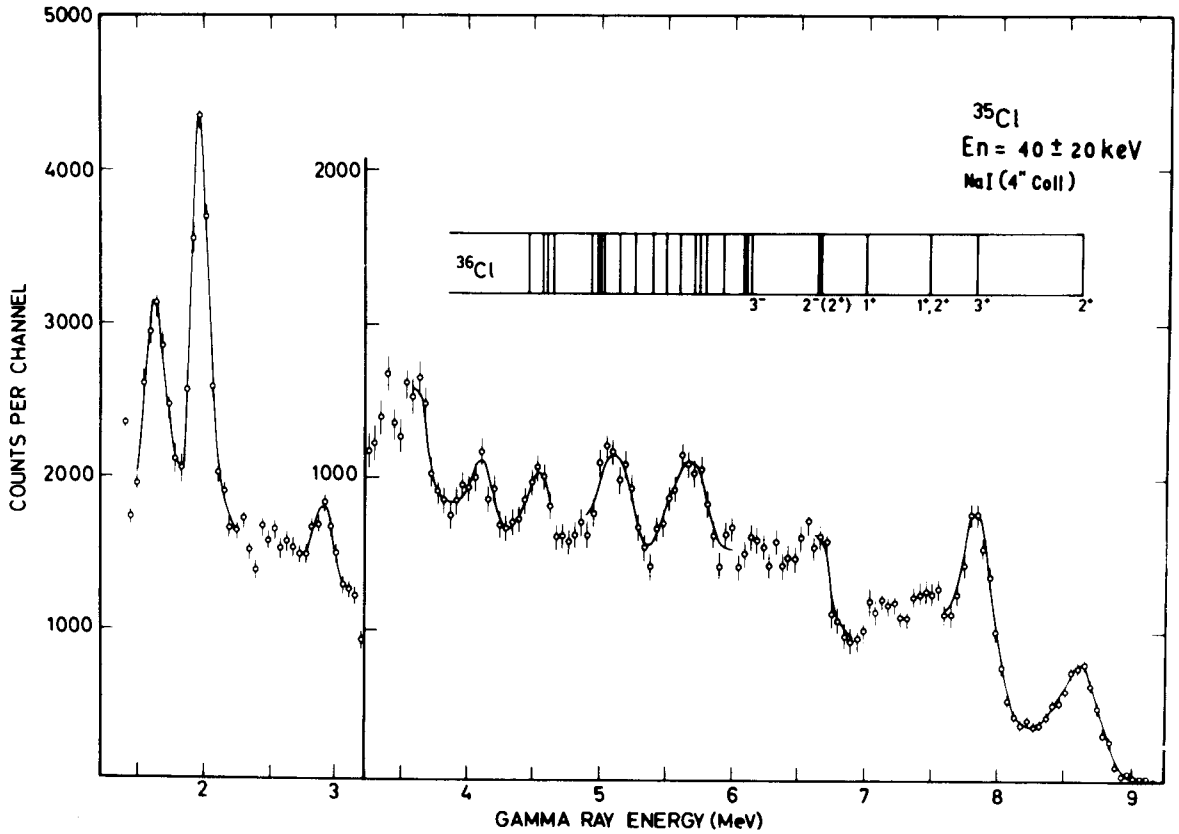

Figure 16 Averaged gamma ray spectrum for capture in ^{35}Cl.

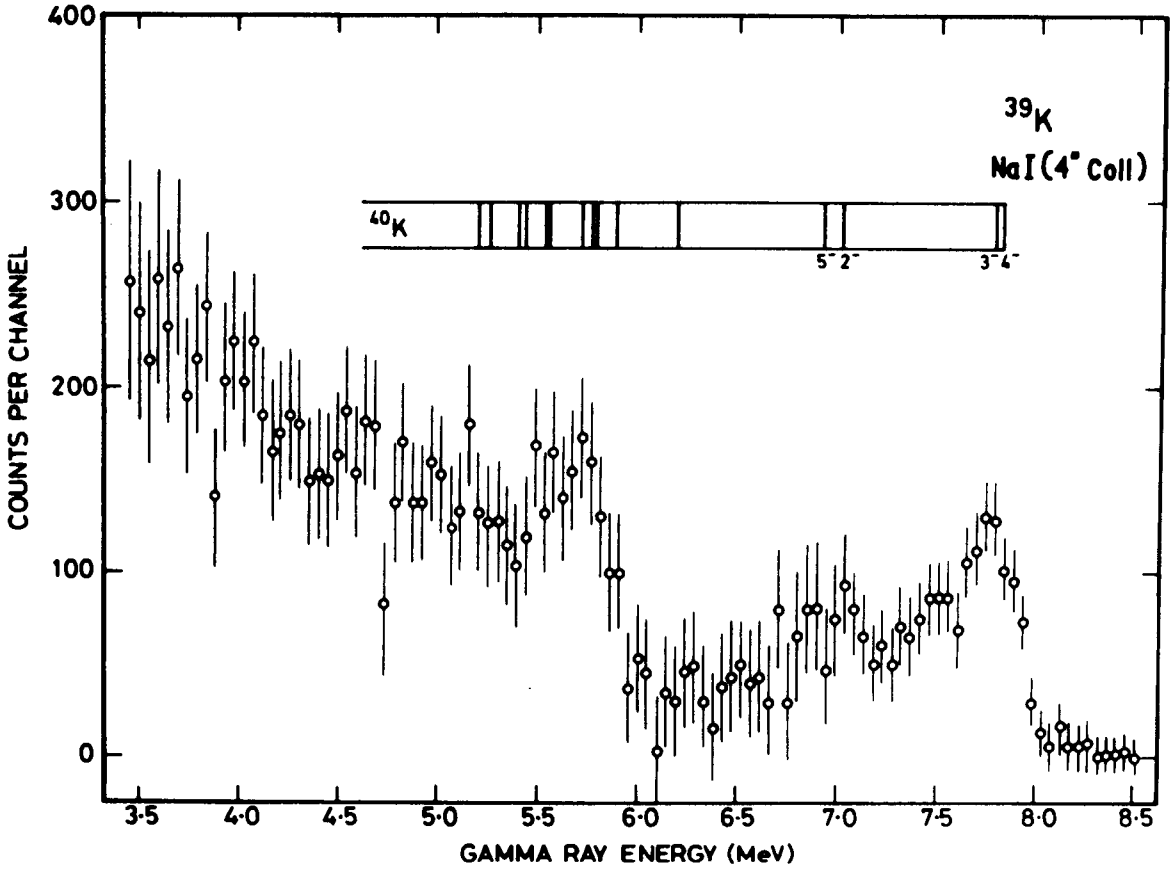

Figure 17 Gamma ray spectrum for capture in ^{39}K.

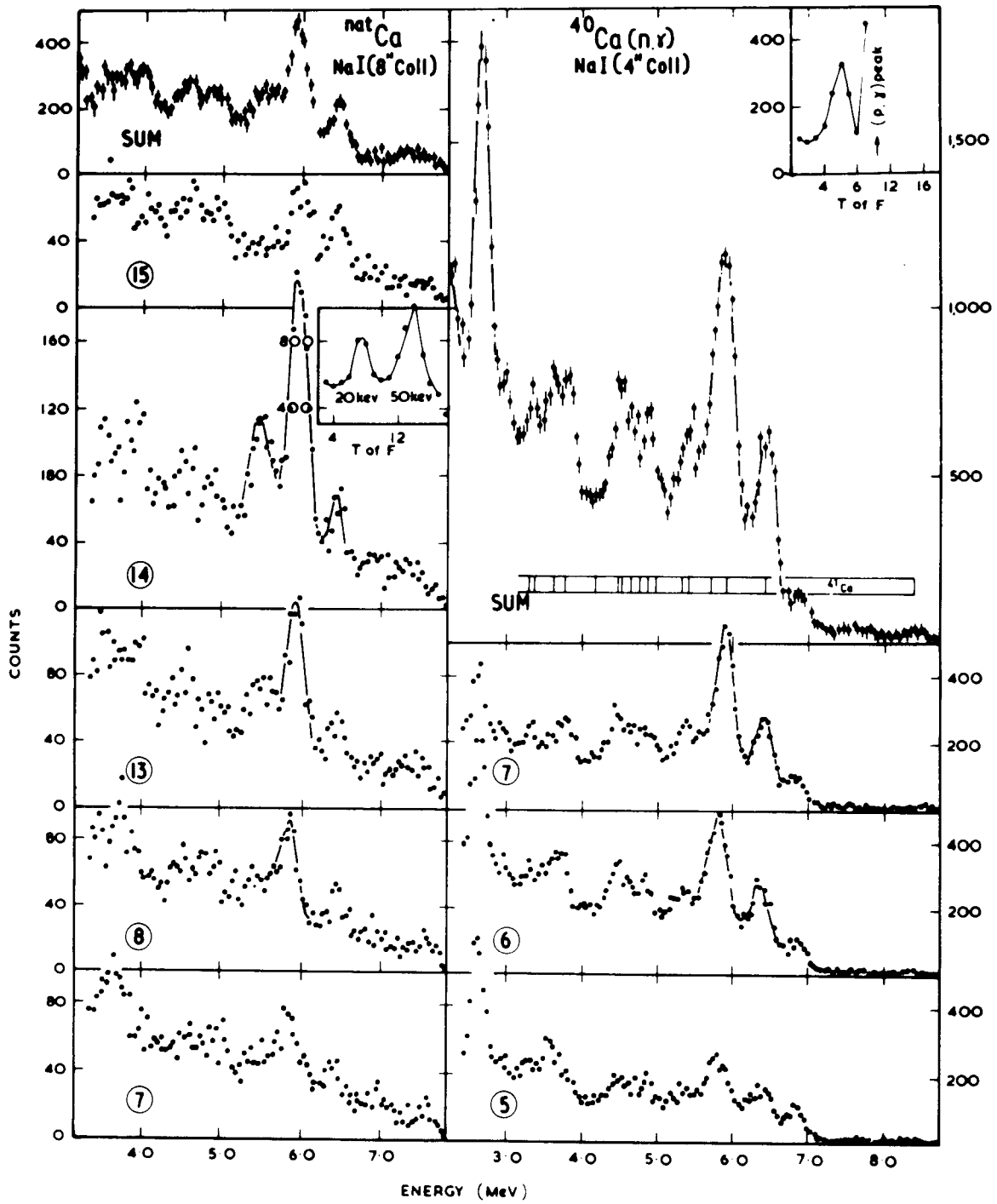

Figure 18 Gamma ray spectra for capture in natural calcium and ^{40}Ca. Circled numerals give neutron time of flight channel for each spectrum (Ref. 14).

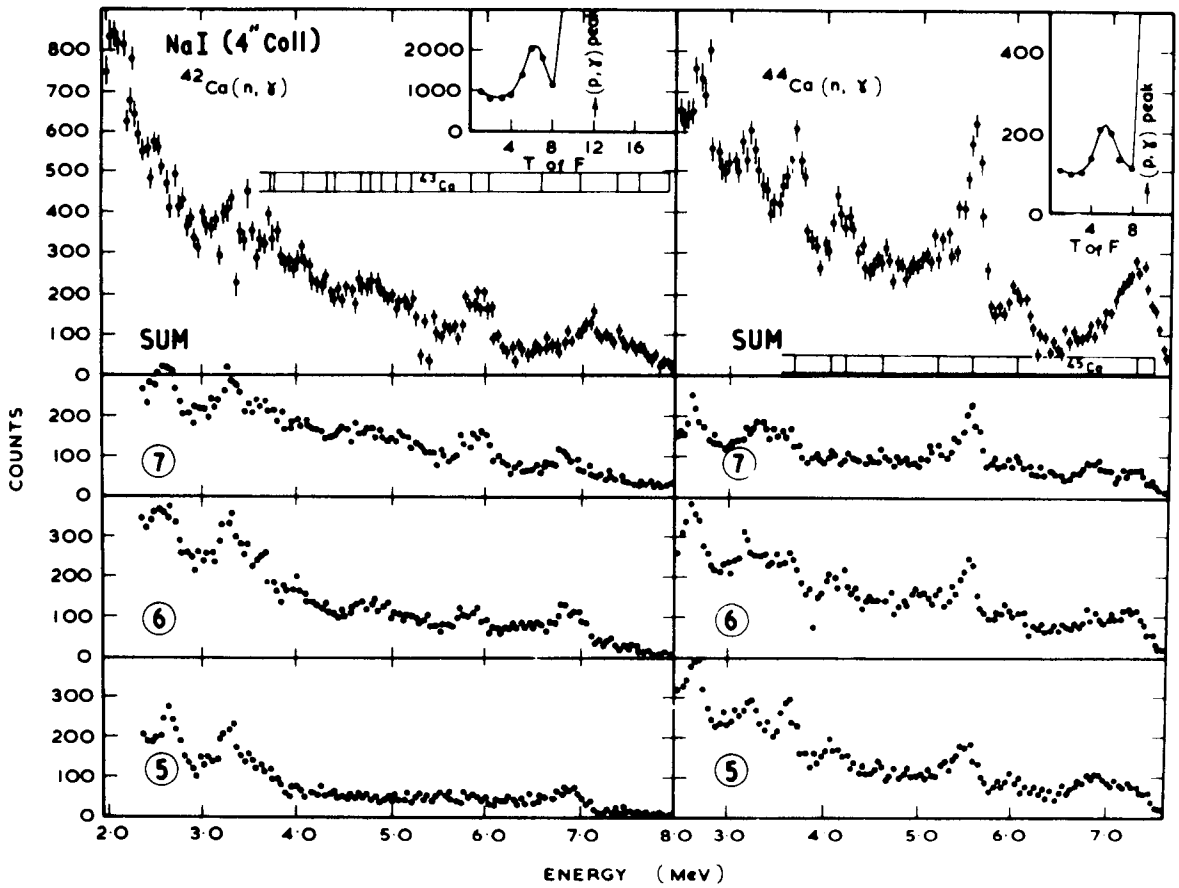

Figure 19 Gamma ray spectra for capture in ^{42}Ca and ^{44}Ca. Circled numerals give neutron time of flight channel for each spectrum (Ref. 14).

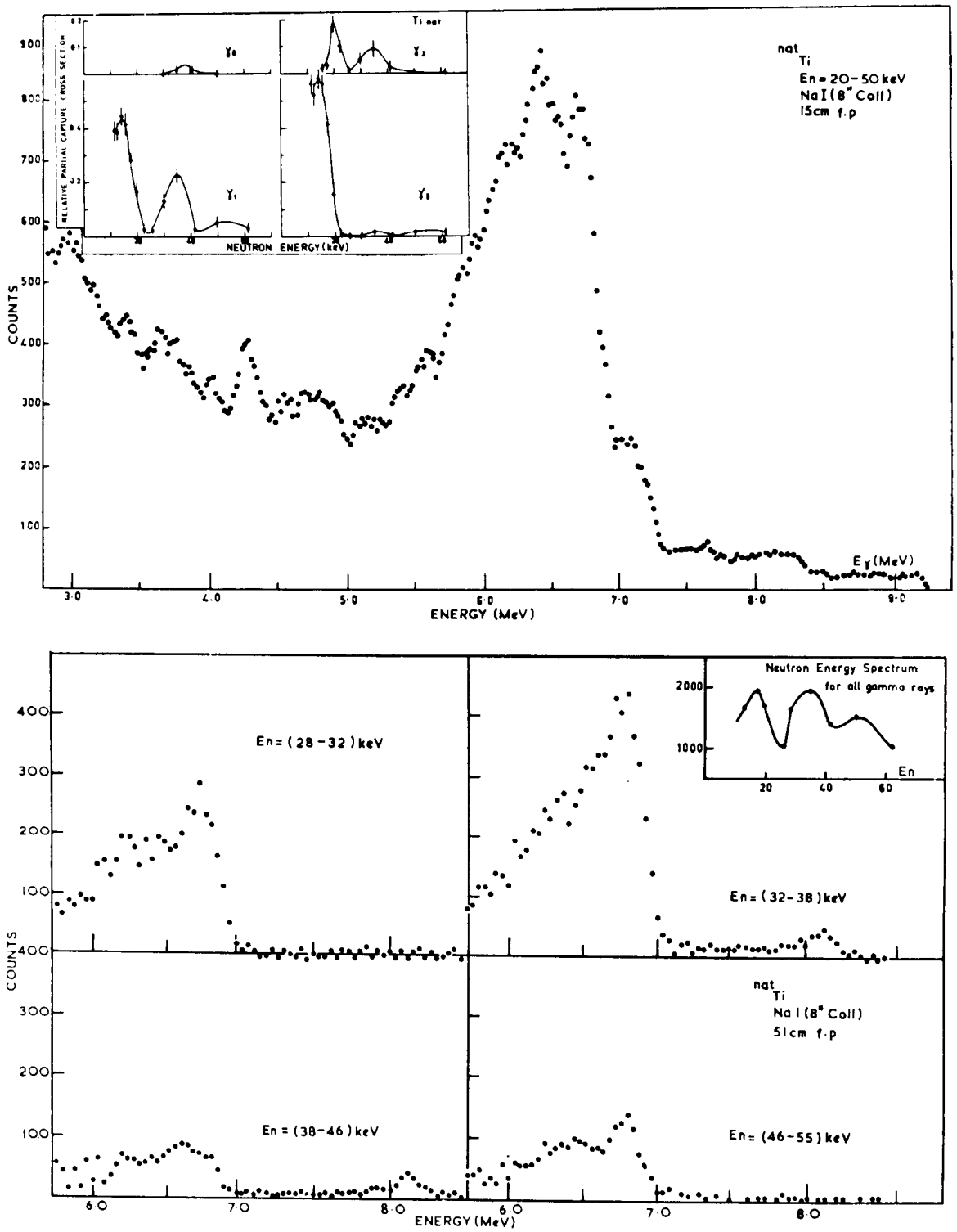

Figure 20 Gamma ray spectra for capture in titanium. Insets give neutron energy dependence of gamma ray intensities. (Ref. 15).

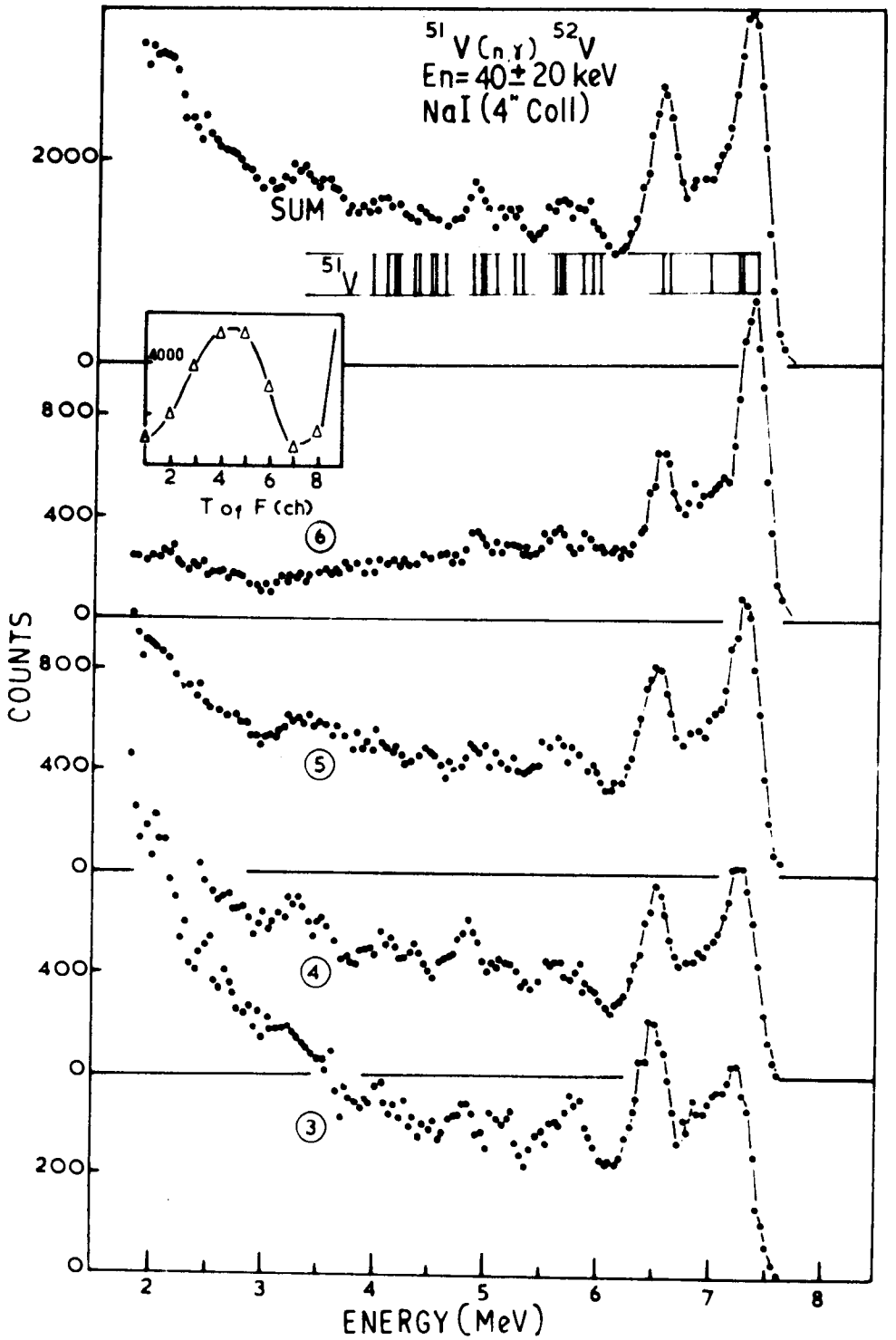

Figure 21 Gamma ray spectrum for capture in vanadium. Circled numerals give neutron time of flight channel for each spectrum.

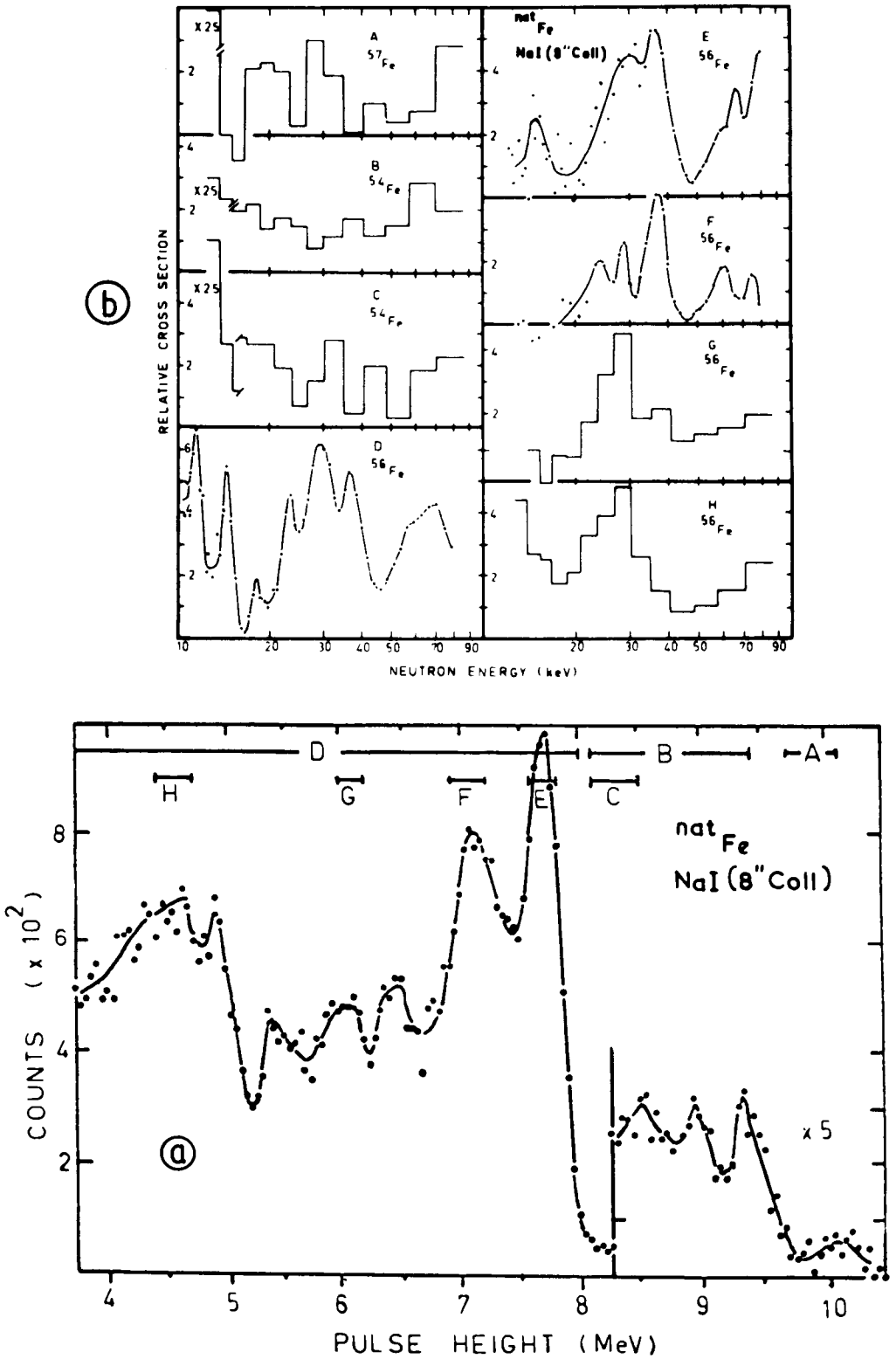

Figure 22 (a) Gamma ray spectrum for capture in iron. Letters show pulse height intervals used for neutron energy spectra.

(b) Neutron energy spectra corrected to give relative partial cross sections.

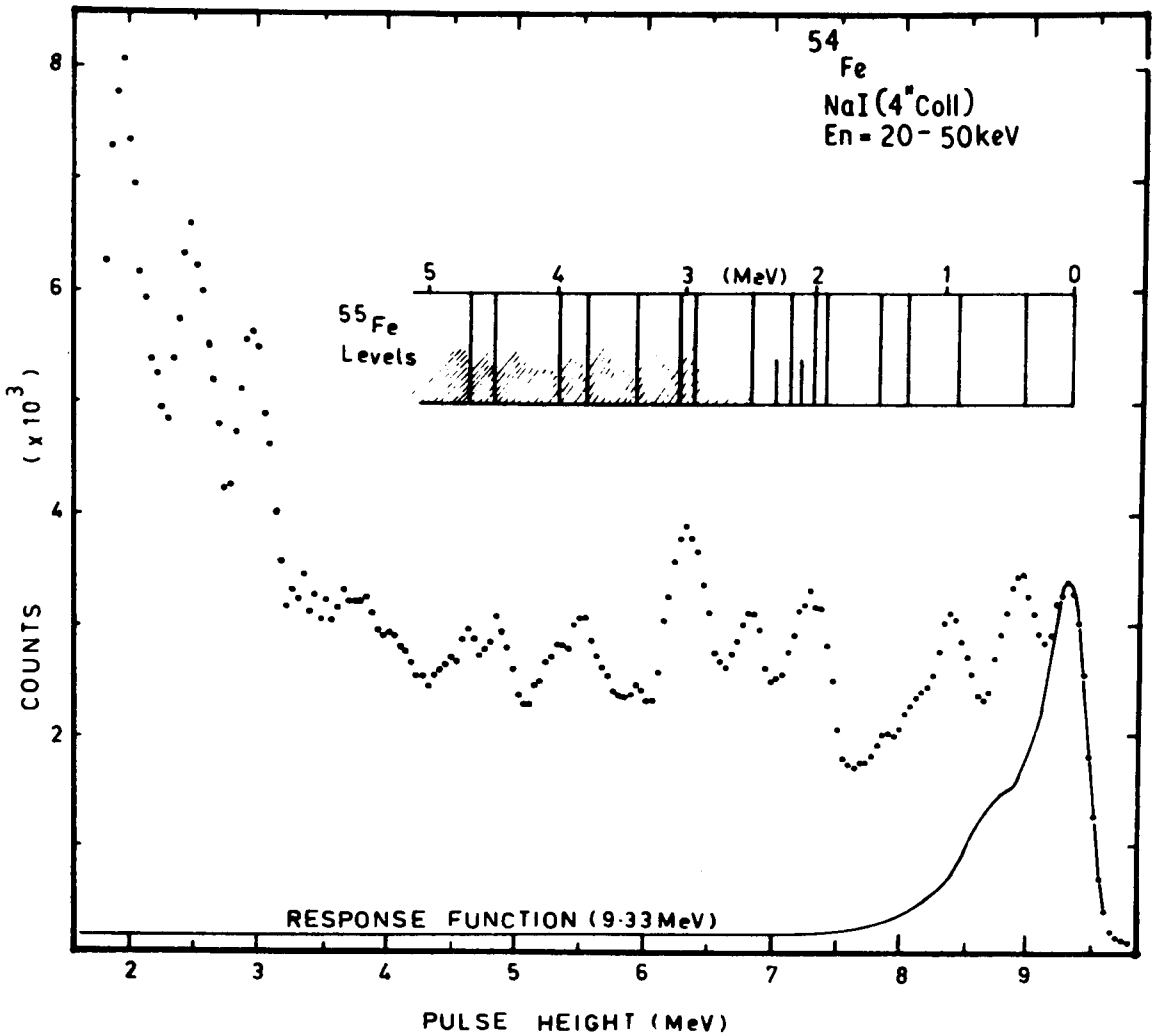

Figure 23 Gamma ray spectrum for capture in ^{54}Fe (Ref. 8).

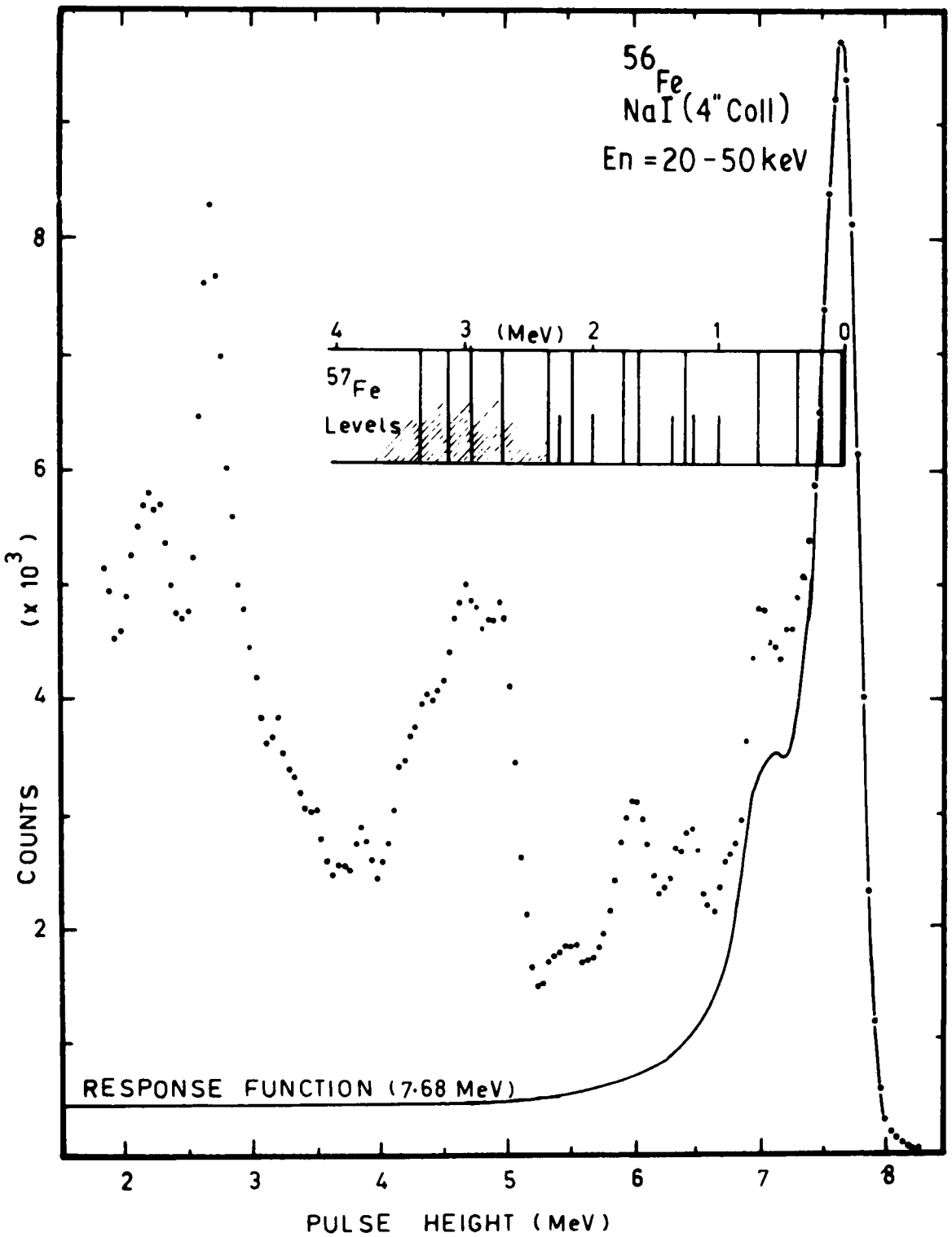

Figure 24 Gamma ray spectrum for capture in ^{56}Fe (Ref. 8).

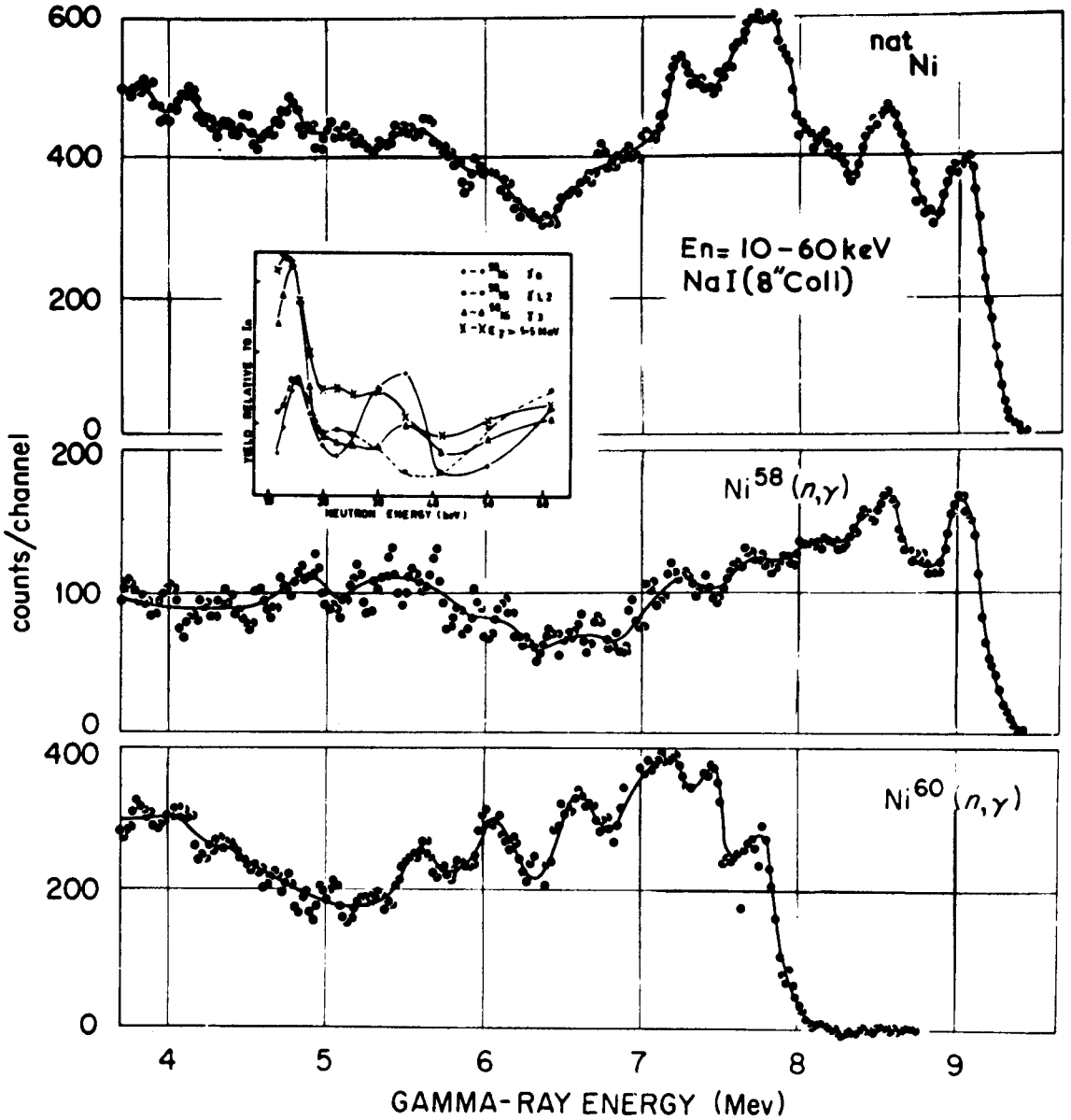

Figure 25 Gamma ray spectra for capture in natural nickel, ^{58}Ni and ^{60}Ni. Inset shows neutron energy dependence of specific γ-ray intensities as a ratio to the yield from an indium target.

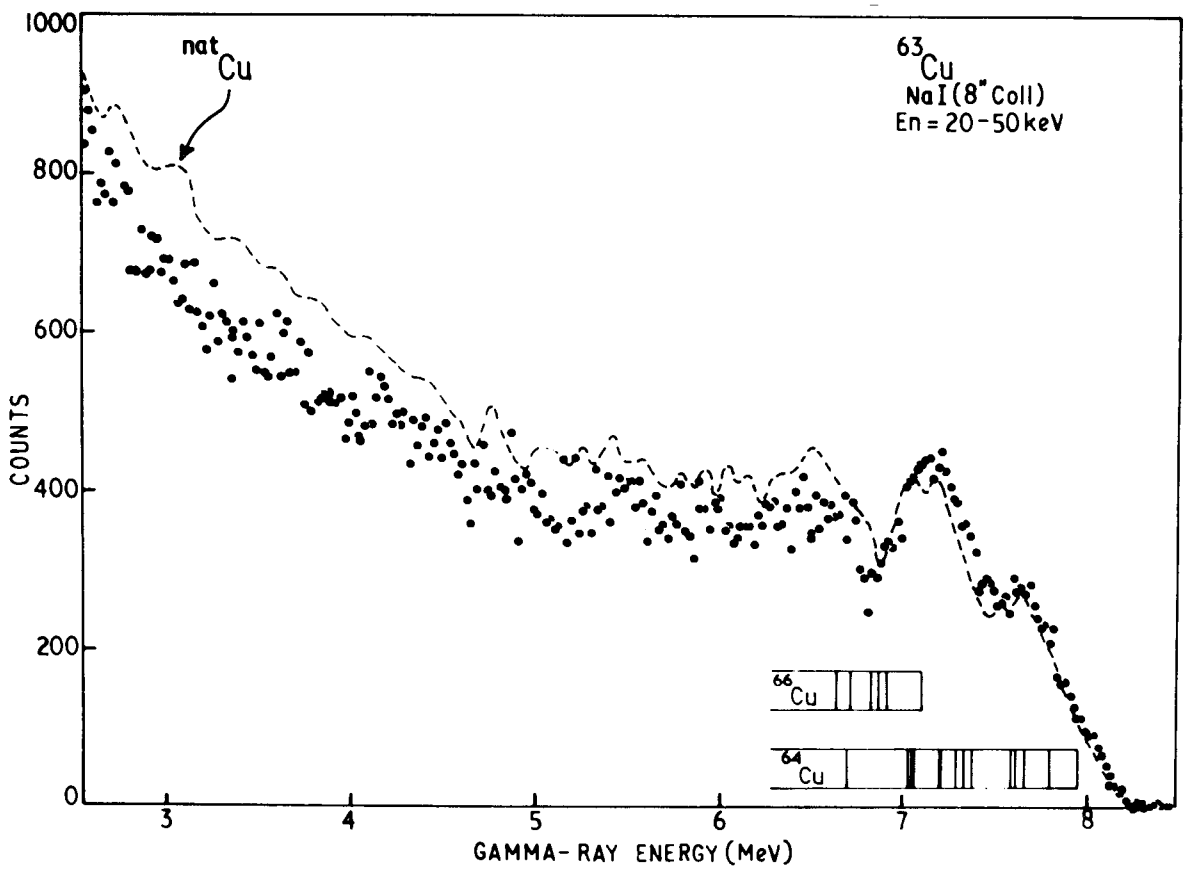

Figure 26 Gamma ray spectra for capture in natural copper and ^{63}Cu.

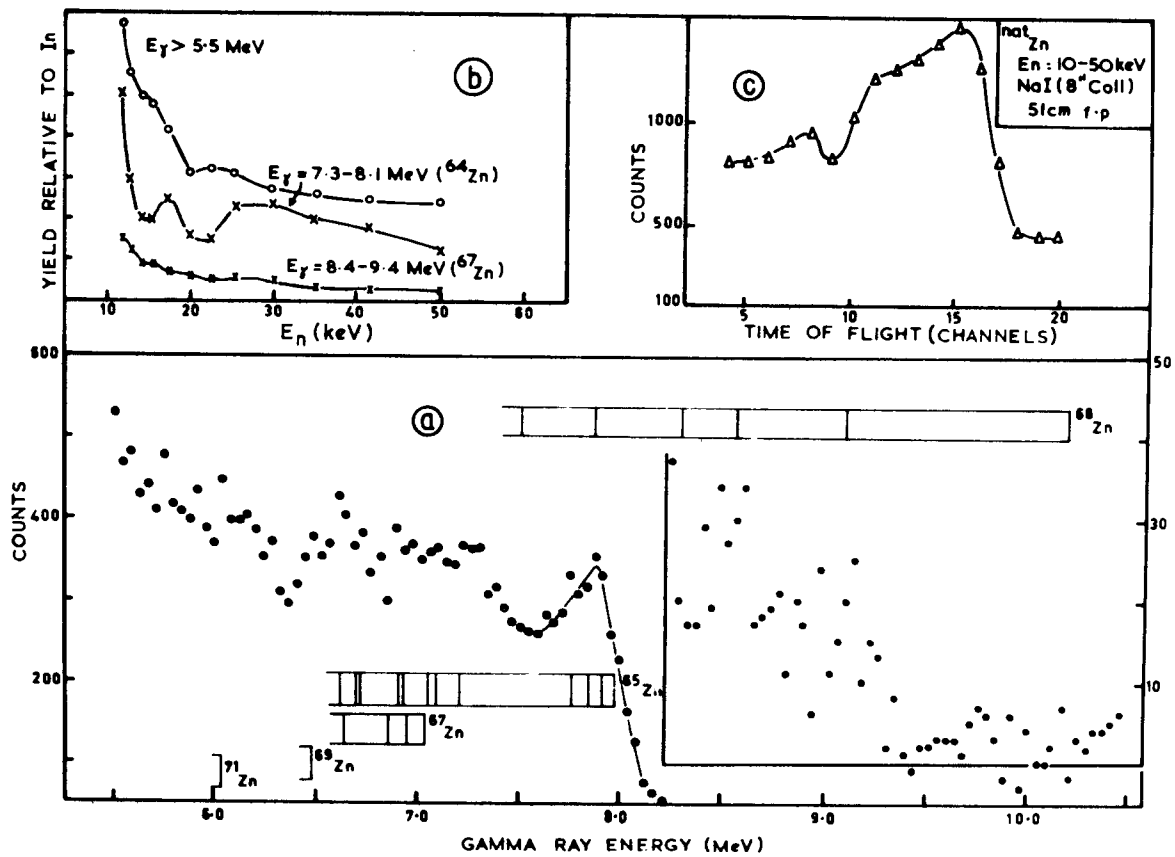

Figure 27 (a) Gamma ray spectrum for capture in zinc (expanded counts scale used above 8.2 MeV).

(b) Neutron energy dependence for particular ranges of E_γ as ratios to the yield from an indium target.

(c) Time of flight spectrum for gamma rays above 5.5 MeV.

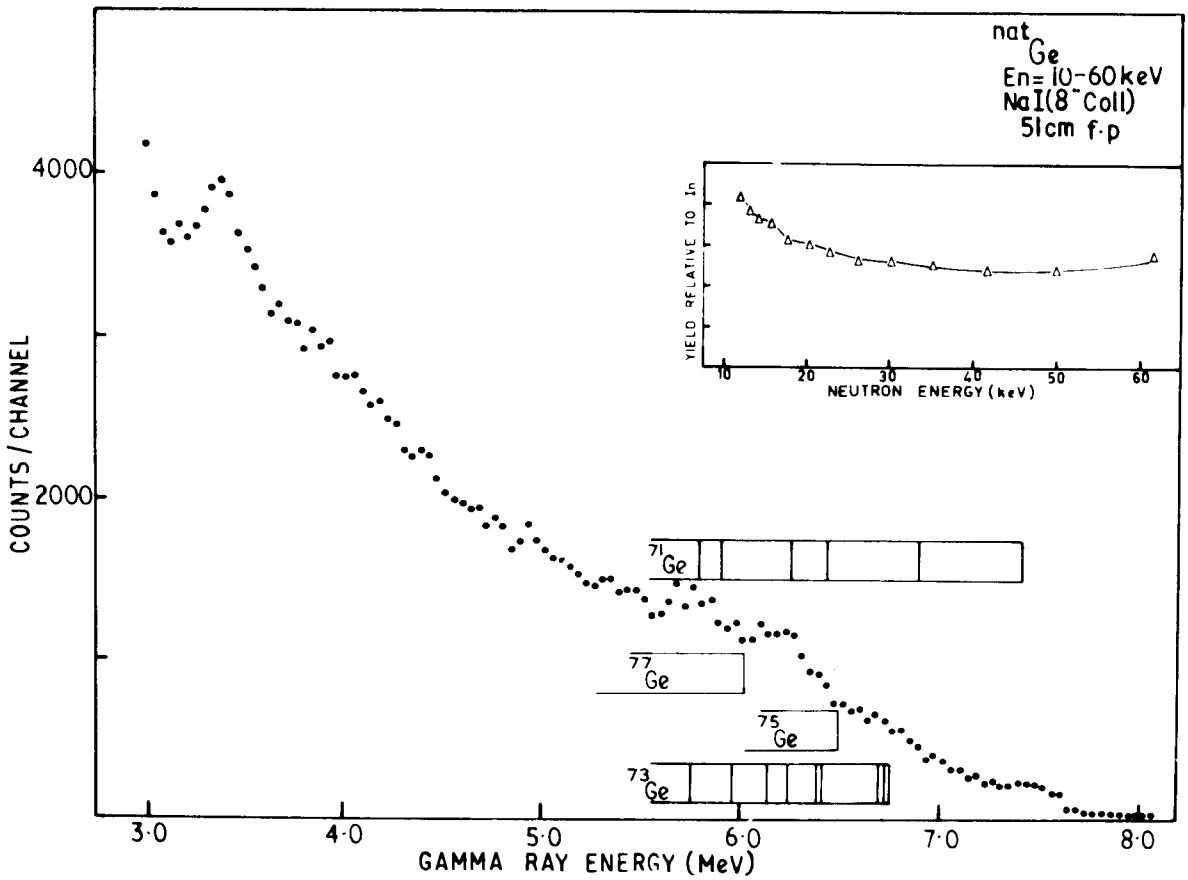

Figure 28 Gamma ray spectrum for capture in germanium. Inset shows neutron energy dependence of gamma ray yield above 3 MeV as a ratio to the yield from an indium target.

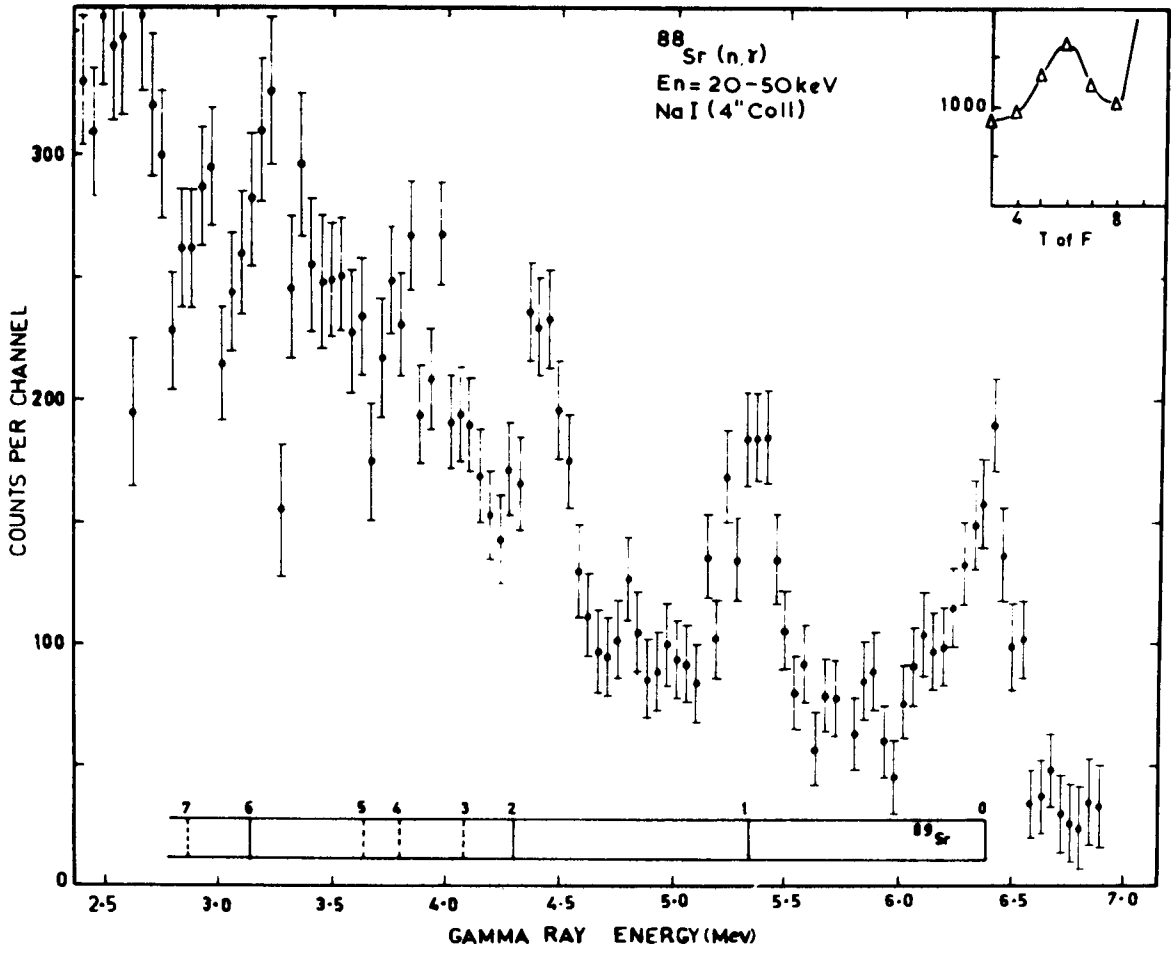

Figure 29 Gamma ray spectrum for capture in ^{88}Sr (Ref. 16).

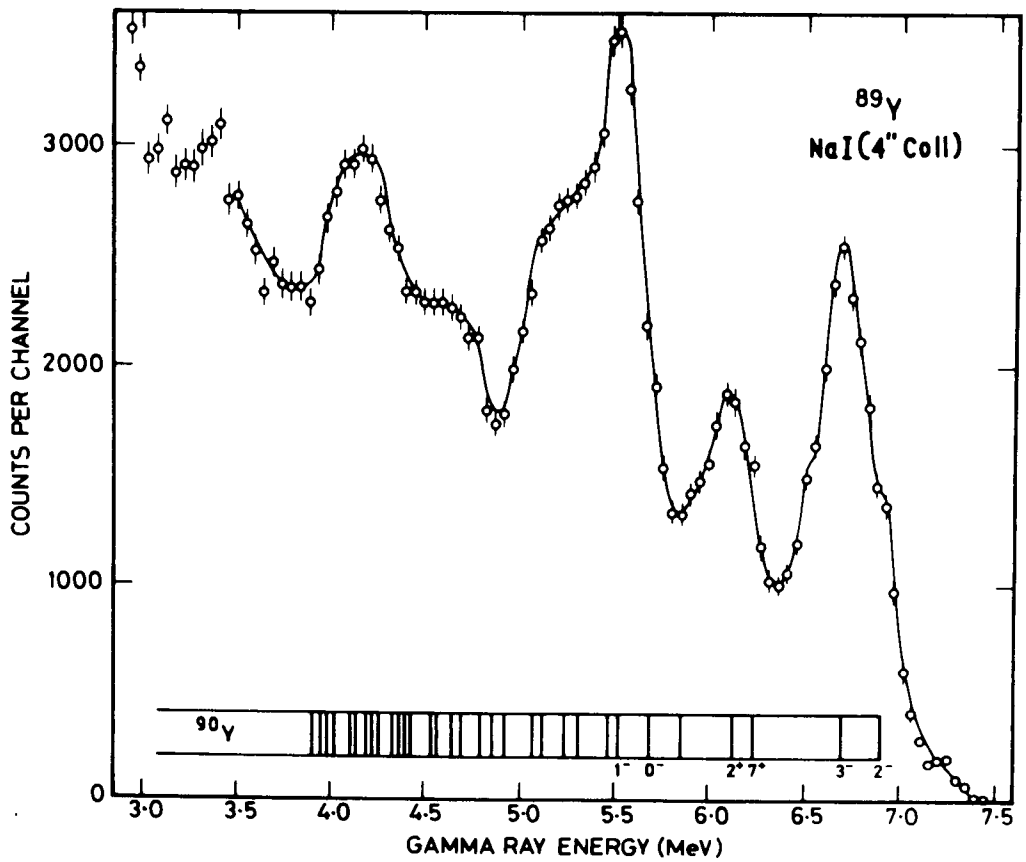

Figure 30 Gamma ray spectrum for capture in yttrium.

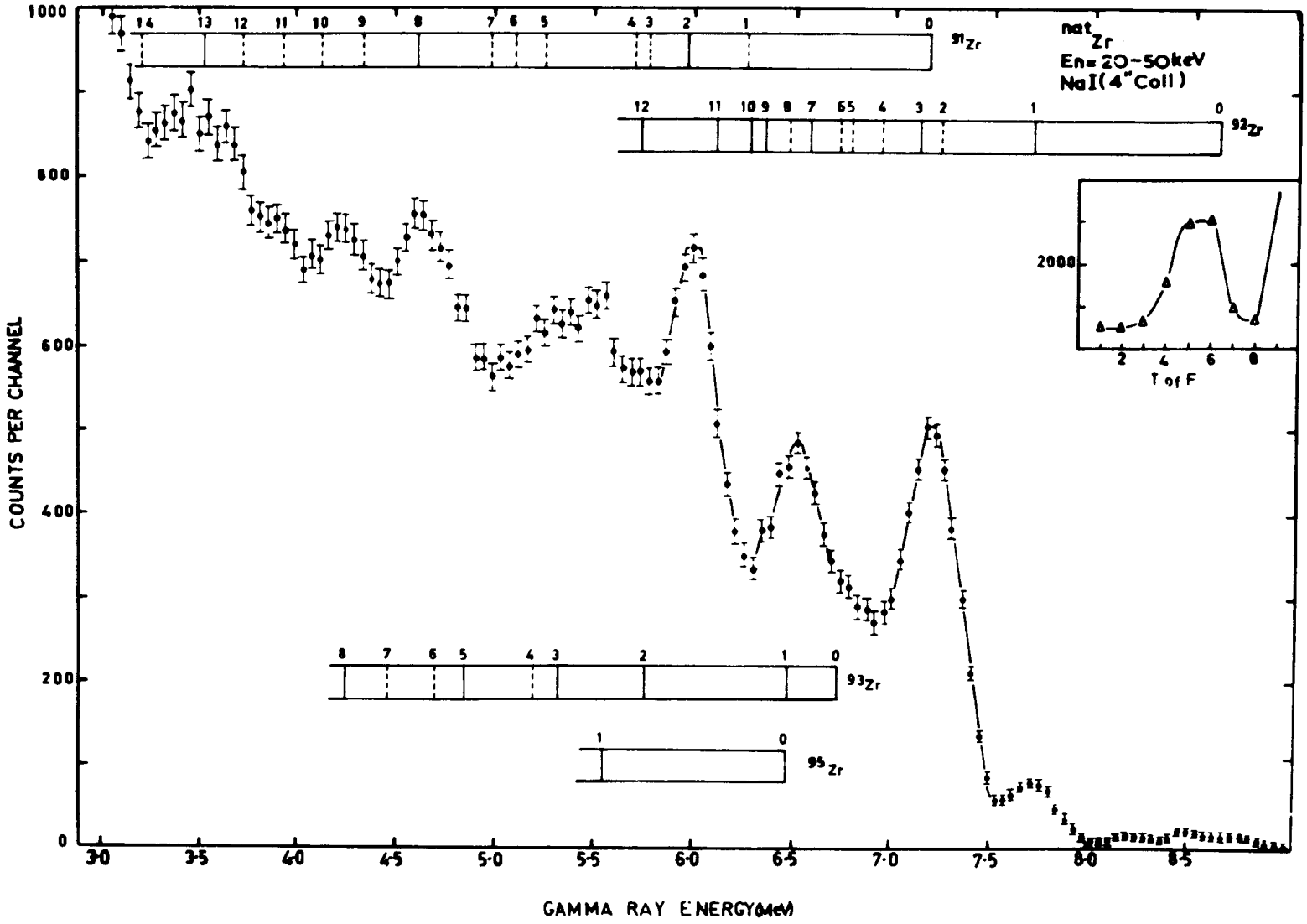

Figure 31 Gamma ray spectrum for capture in zirconium (Ref. 16).

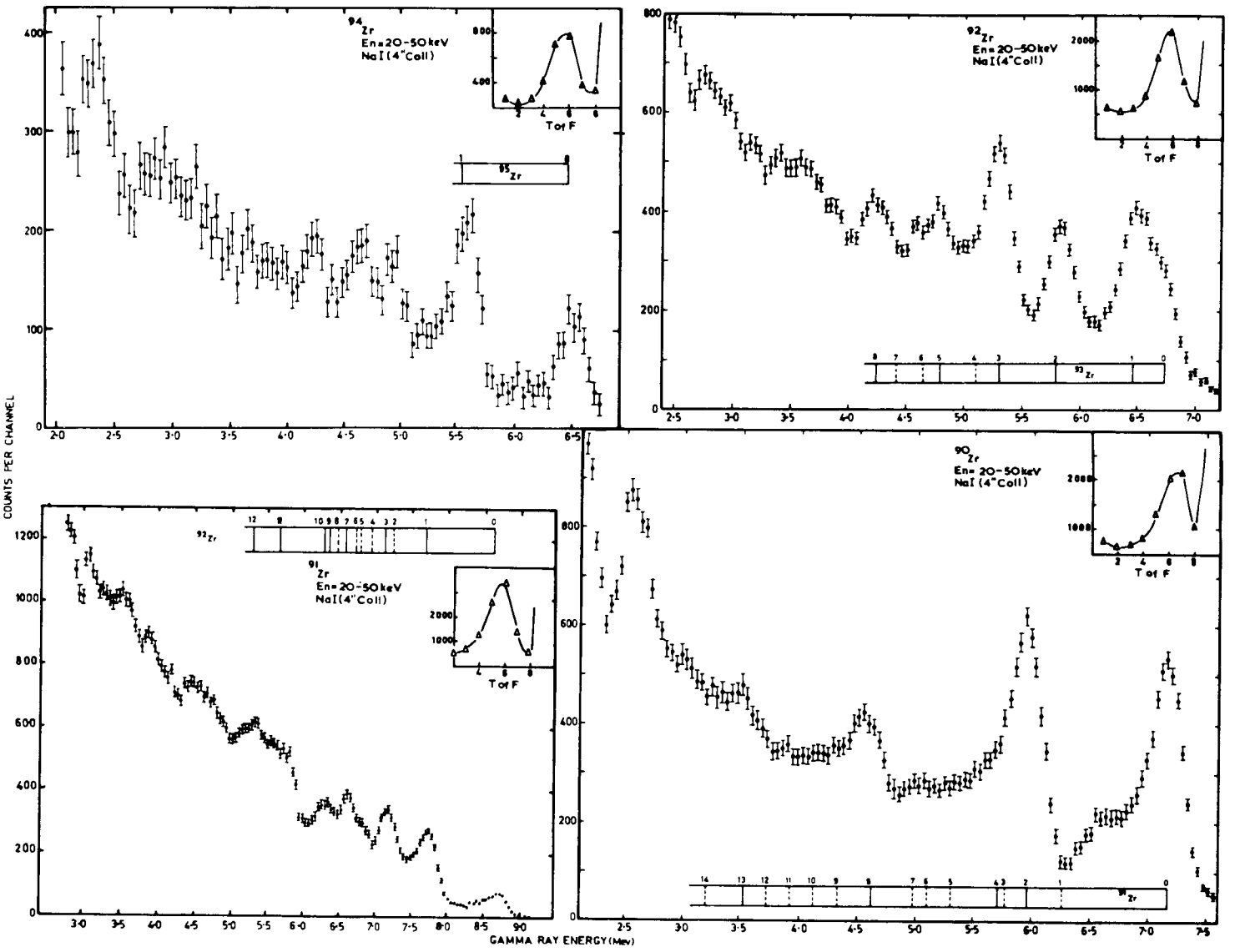

Figure 32 Gamma ray spectra for capture in ^{90}Zr, ^{91}Zr, ^{92}Zr and ^{94}Zr (Ref. 16).

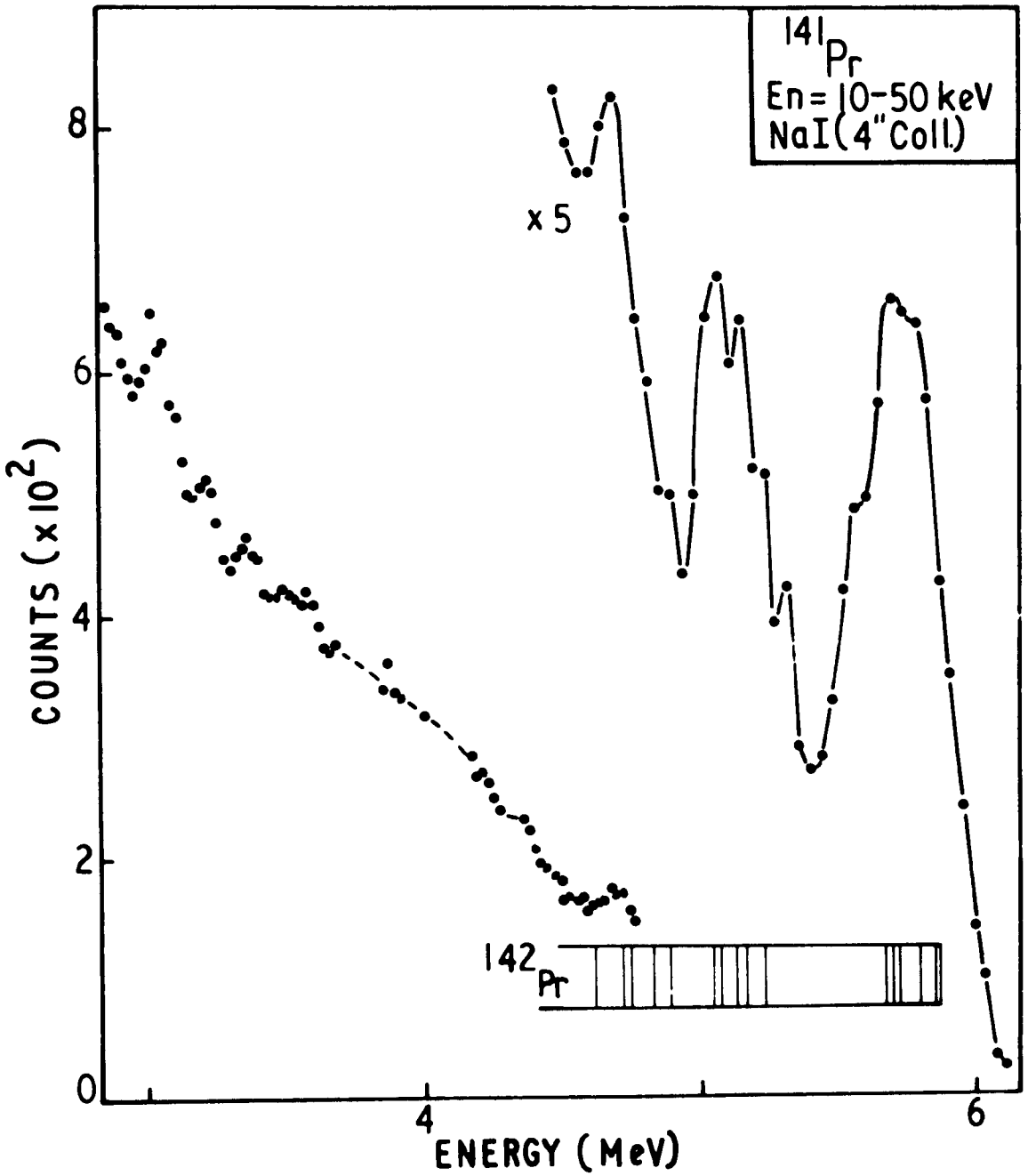

Figure 33 Gamma ray spectrum for capture in praseodymium (Ref. 9).

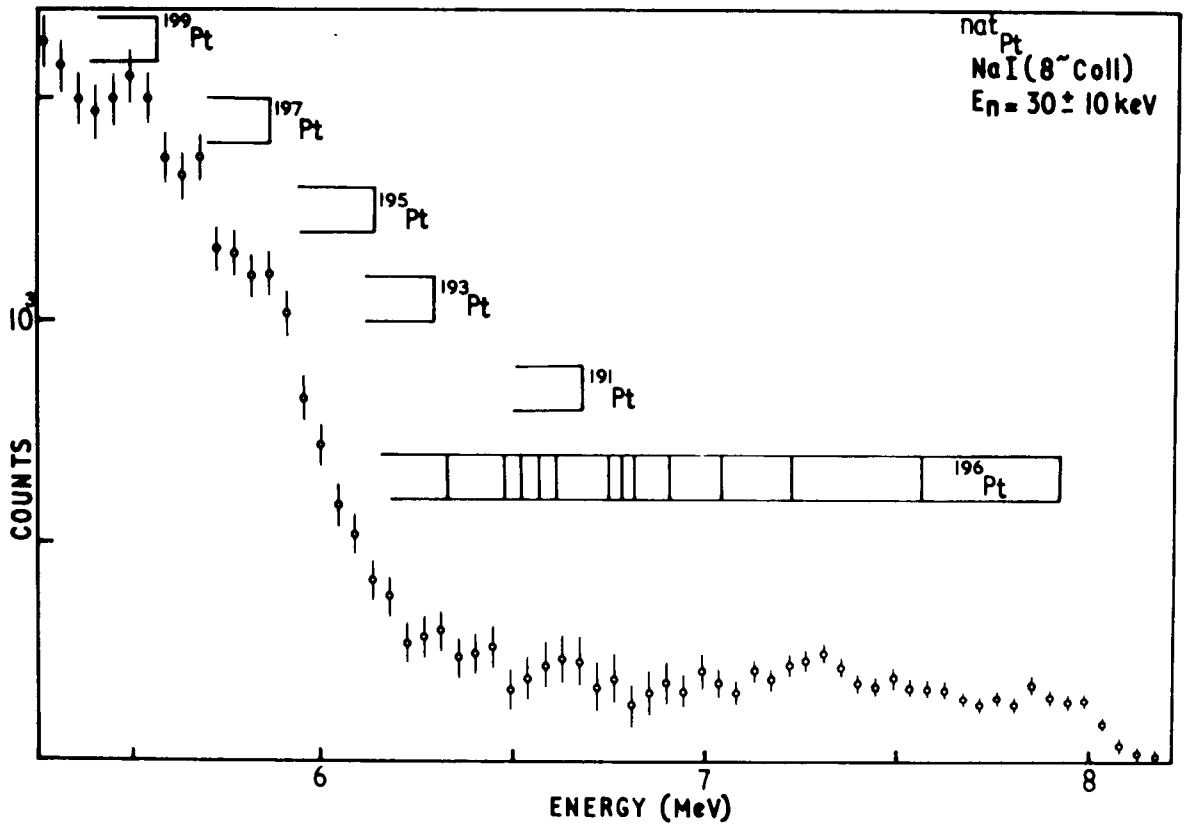

Figure 34 Gamma ray spectrum for capture in platinum (Ref. 9).

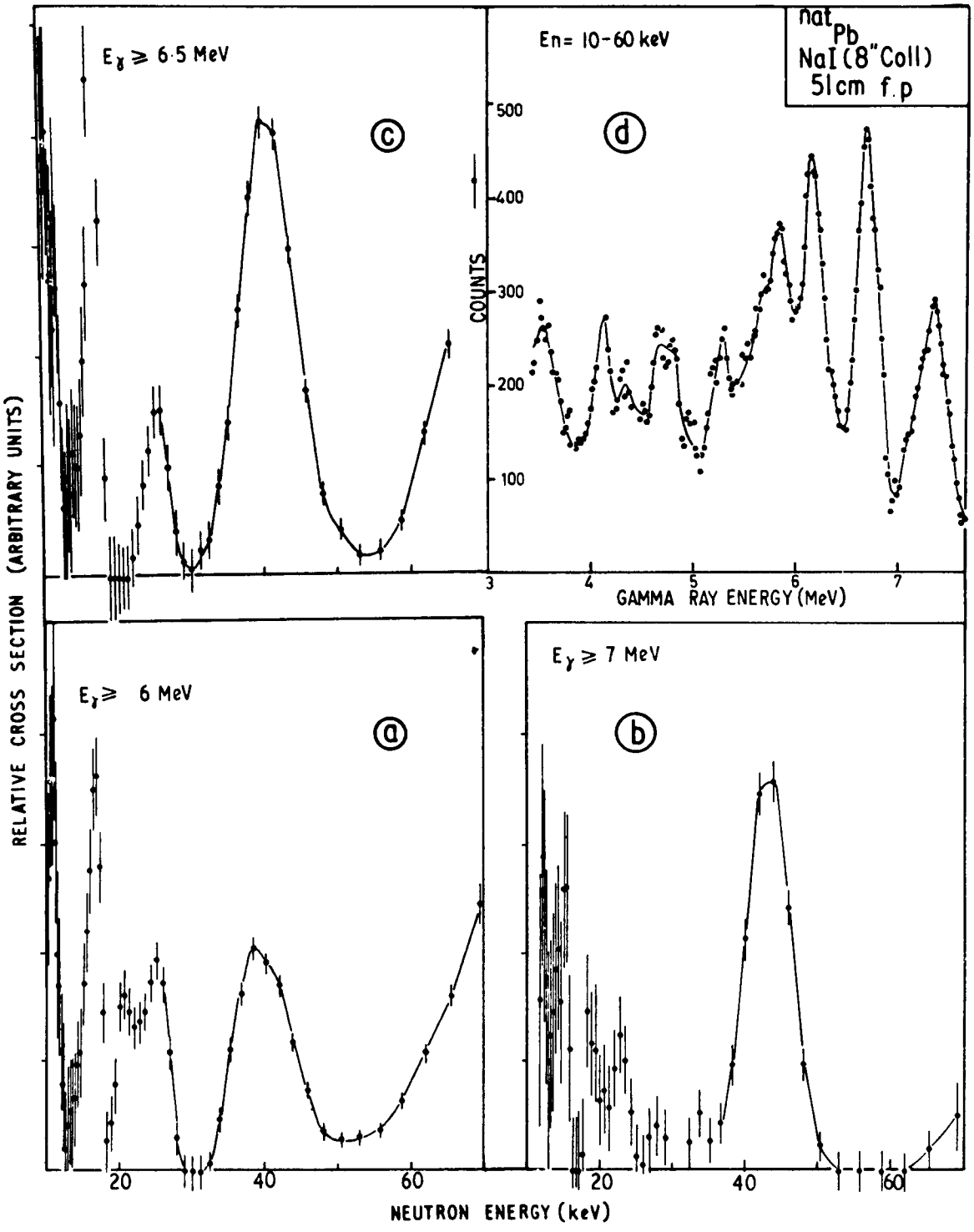

Figure 35 (a), (b) and (c) Neutron energy spectra for lead for specific pulse height intervals, corrected to give relative partial cross sections.

(d) Gamma ray spectrum for capture in lead.

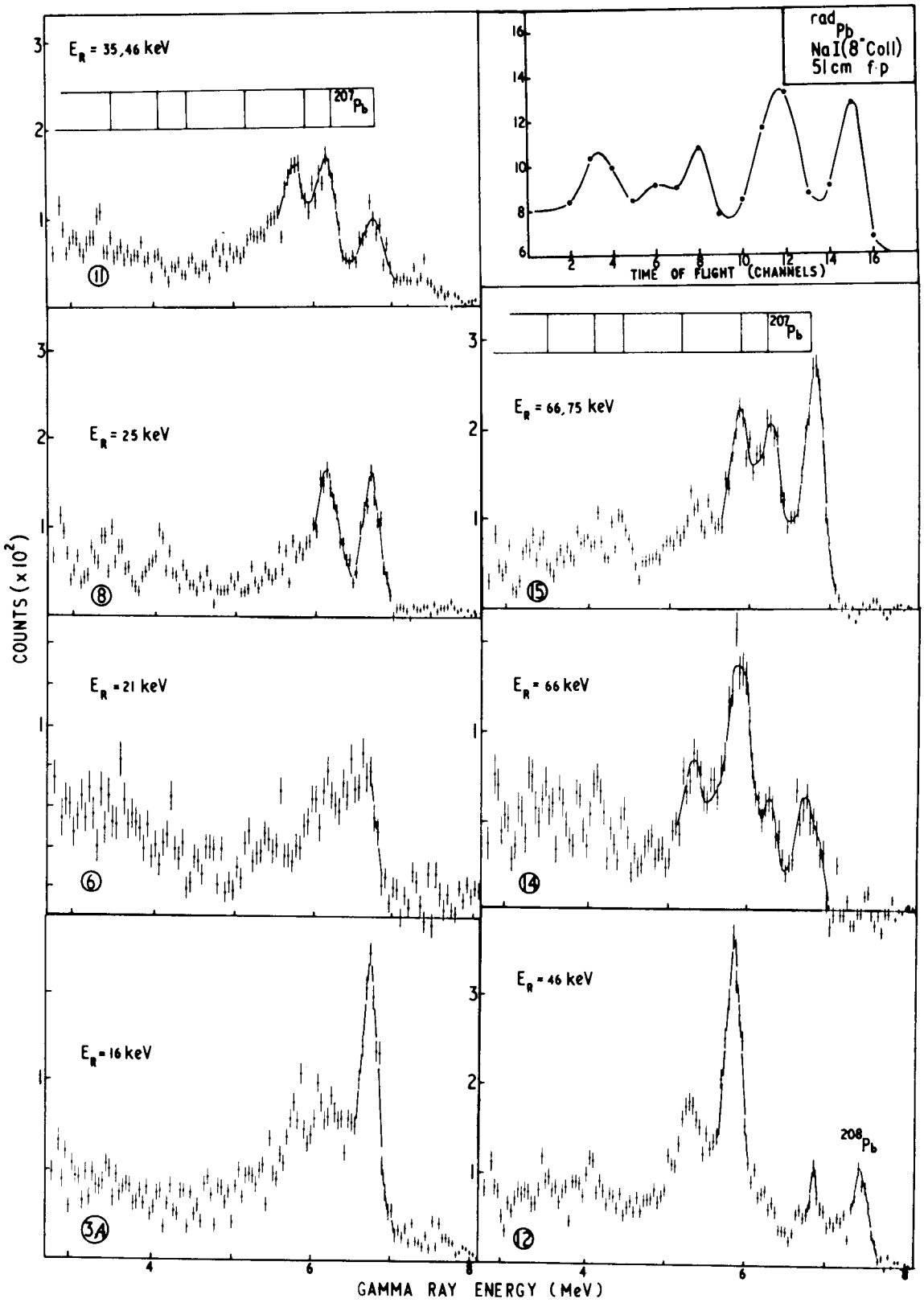

Figure 36 Gamma ray spectra for resonances in radiogenic lead (88% ^{206}Pb). Circled numerals give the neutron time of flight channel for each spectrum.

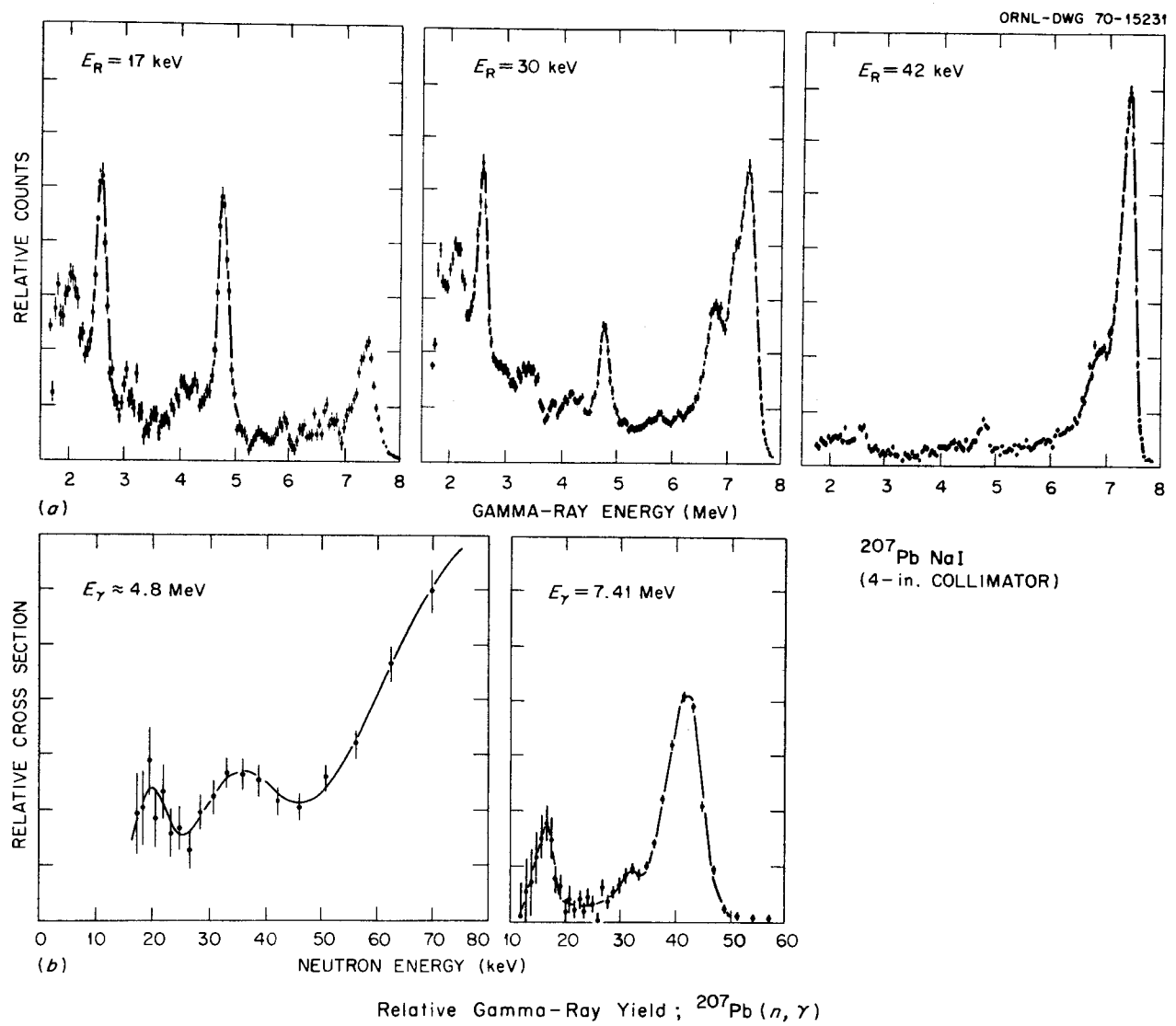

Figure 37 Gamma ray spectra for resonances at 17, 30 and 42 keV in ^{207}Pb.

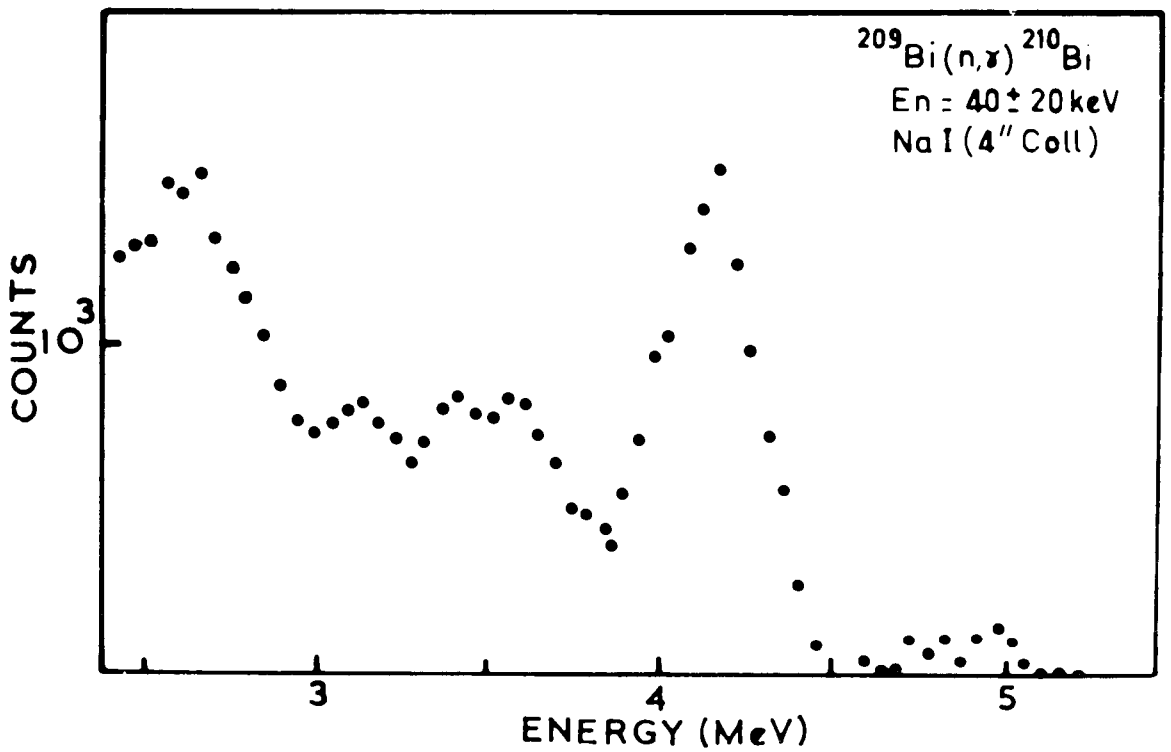

Figure 38 Gamma ray spectrum for capture in bismuth.

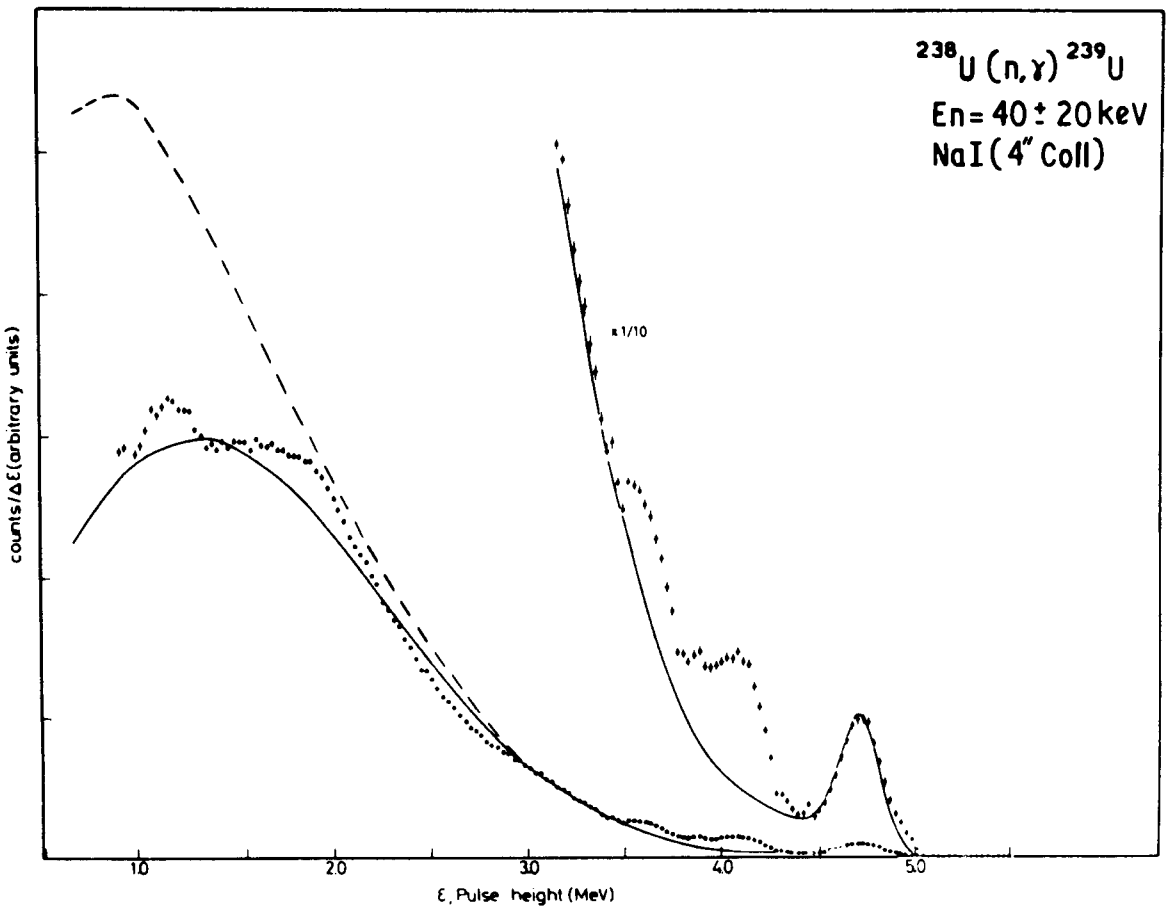

Figure 39 Gamma ray spectrum for capture in ^{238}U (Ref. 12). Dashed curve is theoretical spectrum based on a statistical model. Solid curve is theoretical spectrum as corrected for attenuation in sample and in shield.

FIGURE CAPTIONS

Figure 1 Equipment for measurement of neutron time of flight and gamma ray energy for keV neutron capture.

Figure 2 Resolution (R) and intensity correction factor (K) as a function of gamma ray energy (E_γ).

Figure 3 Typical background pulse height spectrum.

Figure 4 Detector response functions using an 8" collimator.

Figure 5 Detector response functions using a 4" collimator.

Figure 6 Effect of collimating aperture on response function at 7.48 MeV.

Figure 7 Comparison of 7.48 MeV response function and calculation using equation (1).

Figure 8 Variation of pulse height spectrum ratios with gamma ray energy.

Figure 9 Typical neutron time of flight spectra for $E_\gamma > 3$ MeV using a 51 cm flight path.

Figure 10 Gamma ray spectra for resonances at 27 keV and 50 keV in ^{19}F (Ref. 11).

Figure 11 Gamma ray spectrum for the 54 keV resonance in sodium.

Figure 12 Gamma ray spectra for resonances in ^{24}Mg and ^{25}Mg (Refs. 10,11).

Figure 13 Gamma ray spectra for resonances at 35 keV, 89 keV and 120 keV in ^{27}Al (Refs. 10, 11).

Figure 14 Gamma ray spectra for resonances at 30 keV and 111 keV in ^{32}S (Refs. 10, 11).

Figure 15 Gamma ray spectra for neutron energies of 25 keV and 50 keV in ^{35}Cl (Ref. 11).

Figure 16 Averaged gamma ray spectrum for capture in ^{35}Cl.

Figure 17 Gamma ray spectrum for capture in ^{39}K.

Figure 18 Gamma ray spectra for capture in natural calcium and ^{40}Ca. Circled numerals give neutron time of flight channel for each spectrum (Ref. 14).

Figure 19 Gamma ray spectra for capture in ^{42}Ca and ^{44}Ca. Circled numerals give neutron time of flight channel for each spectrum (Ref. 14).

Figure 20 Gamma ray spectra for capture in titanium. Insets give neutron energy dependence of gamma ray intensities. (Ref. 15).

Figure 21 Gamma ray spectrum for capture in vanadium. Circled numerals give neutron time of flight channel for each spectrum.

Figure 22 (a) Gamma ray spectrum for capture in iron. Letters show pulse height intervals used for neutron energy spectra.

(b) Neutron energy spectra corrected to give relative partial cross sections.

Figure 23 Gamma ray spectrum for capture in ^{54}Fe (Ref. 8).

Figure 24 Gamma ray spectrum for capture in ^{56}Fe (Ref. 8).

Figure 25 Gamma ray spectra for capture in natural nickel, ^{58}Ni and ^{60}Ni. Inset shows neutron energy dependence of specific γ-ray intensities as a ratio to the yield from an indium target.

Figure 26 Gamma ray spectra for capture in natural copper and ^{63}Cu.

Figure 27 (a) Gamma ray spectrum for capture in zinc (expanded counts scale used above 8.2 MeV).

(b) Neutron energy dependence for particular ranges of E_γ as ratios to the yield from an indium target.

(c) Time of flight spectrum for gamma rays above 5.5 MeV.

Figure 28 Gamma ray spectrum for capture in germanium. Inset shows neutron energy dependence of gamma ray yield above 3 MeV as a ratio to the yield from an indium target.

Figure 29 Gamma ray spectrum for capture in ^{88}Sr (Ref. 16).

Figure 30 Gamma ray spectrum for capture in yttrium.

Figure 31 Gamma ray spectrum for capture in zirconium (Ref. 16).

Figure 32 Gamma ray spectra for capture in ^{90}Zr, ^{91}Zr, ^{92}Zr and ^{94}Zr (Ref. 16).

Figure 33 Gamma ray spectrum for capture in praseodymium (Ref. 9).

Figure 34 Gamma ray spectrum for capture in platinum (Ref. 9).

Figure 35 (a), (b) and (c) Neutron energy spectra for lead for specific pulse height intervals, corrected to give relative partial cross sections.

(d) Gamma ray spectrum for capture in lead.

Figure 36 Gamma ray spectra for resonances in radiogenic lead (88% ^{206}Pb). Circled numerals give the neutron time of flight channel for each spectrum.

Figure 37 Gamma ray spectra for resonances at 17, 30 and 42 keV in ^{207}Pb.

Figure 38 Gamma ray spectrum for capture in bismuth.

Figure 39 Gamma ray spectrum for capture in ^{238}U (Ref. 12). Dashed curve is theoretical spectrum based on a statistical model. Solid curve is theoretical spectrum as corrected for attenuation in sample and in shield.

SYMBOLS USED IN FIGURES AND TABLES

I_p	Peak current during proton beam pulse
ΔE_p	Incident proton energy (keV) minus threshold energy for $^7Li(p,n)^7Be$ reaction
E_n	Neutron energy (keV)
E_R	Neutron resonance energy (keV)
E_γ	Gamma ray energy (MeV)
t or "T of F"	Neutron time of flight
f.p.	Flight path
4" or 8" Coll.	Measurements made with 4" or 8" diameter collimating aperture in front of the NaI detector
γ_o, γ_1, etc.	Gamma ray transitions to ground state, first excited state, etc. in product nucleus
$I_\gamma(\%)$	Normalized gamma ray intensities (gammas per 100 captures)
E_f	Excitation energy (MeV) of final state reached by gamma ray transition
J_f^π	Spin and parity of final state
J_c^π	Spin and parity of neutron resonance (capturing state)

Distribution

1. Harry Alter, Atomic International
2. R. C. Block, RPI
3. C. D. Bowman, LRL
4. A. D. Carlson, Gulf Gen. Atomic
5. R. E. Chrien, BNL
6. H. Goldstein, Columbia University
7. W. W. Havens, Columbia University
8. H. E. Jackson, ANL
9. H. H. Landon, NBS
10. M. S. Moore, LASL
11. H. W. Newson, Duke University
12. G. C. Phillips, Rice University
13. Alan B. Smith, ANL
14. R. F. Taschek, LASL
15. J. Farrell, LASL
16. R. Hockenbury, RPI
17. H. T. Motz, LASL
18. W. Poenitz, ANL
19. F. B. Simpson, Idaho Nucl. Corp.
20. L. Stewart, LASL
21-30. W. M. Good, ORNL
31. B. J. Allen, ORNL
32-41. I. Bergqvist, LASL
42. L. M. Bollinger, ANL
43. D. H. White, LRL
44. V. Verbinski, Gulf Gen. Atomic
45. V. J. Orphan, Gulf Gen. Atomic
46. N. C. Rasmussen, MIT
47. K. H. Lokan, NRC (Ottawa)
48. G. A. Bartholomew, AECL
49. T. J. Kennett, McMaster University
50-52. E. R. Rae, AERE
53. K. H. Beckhurst, Karlsruhe
54. H. H. Michaelis, Karlsruhe
55. P. M. Endt, Natuurkundig Lab., Utrecht, Netherlands
56. W. Greiner, Universitat Frankfurt AM, Germany
57-106. J. R. Bird, AAEC, Lucas Heights, Australia
107-116. J. A. Biggerstaff, ORNL
117. Gerard de Saussure, ORNL
118. J. K. Dickens, ORNL
119-120. J. L. Fowler, ORNL
121-130. J. H. Gibbons, ORNL
131. J. A. Harvey, ORNL
132. F. K. McGowan, ORNL
133. R. L. Macklin, ORNL
134. P. D. Miller, ORNL
135. R. W. Peelle, ORNL
136. F. G. J. Perey, ORNL

137. G. G. Slaughter, ORNL
138. A. H. Snell, ORNL
139. P. H. Stelson, ORNL
140. A. M. Weinberg, ORNL
141. K. J. Yost, ORNL
142-151. Lab. Records, ORNL
152. ORNL-RC
153-154. DTIE
155-156. Central Research Library
157. Document Reference Section
158. Laboratory and University Div., ORO
159. ORNL Patent Office